11346 *Inorg. Chem.* **2010**, *49*, 11346–11361
DOI: 10.1021/ic100928t

Inorganic Chemistry
Article

Influence of the Synthetic Conditions on the Structural Diversity of Extended Manganese−Oxalato−1,2-bis(4-pyridyl)ethylene Systems

Urko García-Couceiro, Oscar Castillo,* Javier Cepeda, Mónica Lanchas, Antonio Luque, Sonia Pérez-Yáñez, Pascual Román, and Daniel Vallejo-Sánchez

Departamento de Química Inorgánica, Facultad de Ciencia y Tecnología, Universidad del País Vasco, Apartado 644, E-48080 Bilbao, Spain

Received May 10, 2010

We report herein the synthesis and physicochemical characterization of eight new manganese−oxalato compounds with 1,2-bis(4-pyridyl)ethylene (bpe): $\{(Hbpe)_2[Mn_2(\mu\text{-ox})_3]\cdot\sim 0.8(C_2H_5OH)\cdot\sim 0.4(H_2O)\}_n$ (**1**), $\{[Mn(\mu\text{-ox})(\mu\text{-bpe})]\cdot xH_2O\}_n$ (**2**), $[Mn_2(\mu\text{-ox})_2(\mu\text{-bpe})(bpe)_2]_n$ (**3**), $[Mn(\mu\text{-ox})(\mu\text{-bpe})]_n$ (**4a** and **4b**), and $\{[Mn_4(\mu\text{-ox})_3(\mu\text{-bpe})_4(H_2O)_4]\cdot(X)_2\cdot mY\}_n$ with X = NO_3^- (**5a**), Br^- (**5b**), and ClO_4^- (**5c**) and Y = solvation molecules. The appropriate selection of the synthetic conditions allowed us to control the crystal structure and to design extended 2D and 3D frameworks. Compound **1** is obtained at acid pH values and its crystal structure consists of stacked $[Mn_2(\mu\text{-ox})_3]^{2-}$ layers with cationic $Hbpe^+$ molecules intercalated among them. Compound **2** was obtained at basic pH values with a manganese/bpe ratio of 1:1, and the resulting 3D structure consists of an interpenetrating framework in which metal−oxalato chains are bridged by bpe ligands, leading to a microporous network that hosts a variable number of water molecules (between 0 and 1) depending on the synthetic conditions. Compound **3**, synthesized with a manganese/bpe ratio of 1:3, shows a 2D framework in which linear metal−oxalato chains are joined by bis-monodentate 1,2-bis(4-pyridyl)ethylene ligands. The thermal treatment of compound **3** permits the release of one of the bpe molecules, giving rise to two new 2D crystalline phases of formula $[Mn(\mu\text{-ox})(\mu\text{-bpe})]_n$ (**4a** and **4b**) depending on the heating rate. The open structures of **5a**−**5c** were synthesized in a medium with a high concentration of nitrate, perchlorate, or bromide salts (potassium or sodium as cations). These anions behave as templating agents directing the crystal growing toward a cationic porous network, in which the anions placed in the voids and channels of the structure present high mobility, as inferred from the ionic exchange experiments. Variable-temperature magnetic susceptibility measurements show an overall antiferromagnetic behavior for all compounds, which are discussed in detail.

Intoduction

Metal−organic coordination polymers have attracted considerable interest because of their promising properties and applications in areas such as catalysis, zeolitic behavior, electrical conductivity, luminescence, nonlinear optics, and magnetism.[1] The rational design of new compounds with novel topologies and specific chemical and physical properties comprises the basis and purpose of crystal engineering and involves a good understanding of the metal ion, the coordination preferences of the bridging entities, and the supramolecular self-assembly by noncovalent interactions for the development of new strategies for the synthesis of these materials.[2] Carboxylates are interesting ligands for this goal because of their versatile coordination modes and high structural stability, which has allowed the synthesis of compounds ranging from discrete oligonuclear species to one-, two-, and three-dimensional networks.[3] Moreover, organic carboxylate linkers and pillared polypyridines have been demonstrated to be very efficient in the construction of 3D open metal−organic frameworks (MOFs). The wall of channels can be easily functionalized, and their size can be systematically expanded without changing the underlying

*To whom correspondence should be addressed. Fax: (internat) +34-94601-3500. E-mail: oscar.castillo@ehu.es.

(1) (a) James, S. L. *Chem. Soc. Rev.* **2003**, *32*, 276. (b) Janiak, C. *J. Chem. Soc., Dalton Trans.* **2003**, 2781. (c) Kitagawa, S.; Kitaura, R.; Noro, S. *Angew. Chem., Int. Ed.* **2004**, *43*, 2334. (d) Rowsell, J. L. C.; Yaghi, O. M. *Microporous Mesoporous Mater.* **2004**, *73*, 3. (e) Férey, G. *Chem. Soc. Rev.* **2008**, *37*, 191. (f) Ma, L.; Abney, C.; Lin, W. *Chem. Soc. Rev.* **2009**, *38*, 1248. (g) Czaja, A. U.; Trukhan, N.; Müller, U. *Chem. Soc. Rev.* **2009**, *38*, 1284. (h) Allendorf, M. D.; Bauer, C. A.; Bhakta, R. K.; Houk, R. J. T. *Chem. Soc. Rev.* **2009**, *38*, 1330. (i) Kurmoo, M. *Chem. Soc. Rev.* **2009**, *38*, 1353. (j) Lee, J. Y.; Farha, O. K.; Roberts, J.; Scheidt, K. A.; Nguyen, S. T.; Hupp, J. T. *Chem. Soc. Rev.* **2009**, *38*, 1450. (k) Li, J.-R.; Kuppler, R. J.; Zhou, H.-C. *Chem. Soc. Rev.* **2009**, *38*, 1477. (l) Chen, B.; Xiang, S.; Qian, G. *Acc. Chem. Res.* **2010**, *43*, 1115.

(2) (a) Holliday, B. J.; Markin, C. A. *Angew. Chem., Int. Ed.* **2001**, *40*, 2022. (b) Lehn, J.-M. *Science* **2002**, *295*, 2400. (c) Brammer, L. *Chem. Soc. Rev.* **2004**, *33*, 476. (d) Trnchemontagne, D. J.; Mendoza-Cortés, J. L.; O'Keefe, M.; Yaghi, O. M. *Chem. Soc. Rev.* **2009**, *38*, 1257. (e) Perry, J. J., IV; Perman, J. A.; Zaworotko, M. J. *Chem. Soc. Rev.* **2009**, *38*, 1400.

(3) (a) Rao, C. N. R.; Natarajan, S.; Vaidhyanathan, R. *Angew. Chem., Int. Ed.* **2004**, *43*, 1466. (b) Eddaoudi, M.; Moler, D. B.; Li, H.; Chen, B.; Reineke, T. M.; O'Keeffe, M.; Yaghi, O. M. *Acc. Chem. Res.* **2001**, *34*, 319.

 Published on Web 11/19/2010

topology, showing really interesting storage[4] and catalytic[5] properties.

The rigid bridging oxalato ligand (hereafter abbreviated as ox) has appeared as a very appealing tecton in the construction of a great diversity of homo- and heterometallic compounds with interesting physical properties (magnetic, electric, or optical), due to its ability to mediate electronic effects between paramagnetic centers.[6] The prevalence of its rigid bis-chelating bridging mode provides a degree of predictability with regard to the structural motifs and architectures of the resulting coordination networks. It is well-known that the counterions can exert a template effect on the topology and dimensionality of the oxalato-bridged polymeric networks. Compounds of general formula $[M^{II}_2(\mu\text{-ox})_3]^{2-}$ or $[M^{II}M^{III}(\mu\text{-ox})_3]^{-}$ (M^{II} = V, Cr, Mn, Fe, Co, Ni, Cu, Zn; M^{III} = V, Cr, Fe) form 2D honeycomb layers with voluminous achiral cations,[7] whereas helical 3D networks are obtained if chiral tris-chelated transition-metal diimine complexes $[M(L)_3]^{m+}$ (L = 2,2′-bipyridine or phenantroline; m = 2, 3) are used.[8]

The features of the auxiliary organic ligands used to complete the metal coordination sphere also play an important role in the dimensional control of these polymeric compounds. Thus, discrete oligonuclear species have been obtained using multidentate N- and/or O-donor flexible ligands that block most of the coordination sites of the metal.[9] In our previous research, we designed 1D and 2D complexes of the formula $[M(\mu\text{-ox})(L)_x]_n$ (M(II) = Mn, Fe, Co, Ni, Cu, Zn; x = 1, 2; L = terminal ligand) in which aromatic pyridyl moieties,[10] triazole derivatives,[11] or nucleobases[12] behave as monodentate terminal ligands providing 1D linear or *zigzag* frameworks and 4,4′-dipyridyl derivatives which connect the metal−oxalato chains, forming sheets.[13]

However, the synthetic conditions (reactants, pH, temperature, concentration, stoichiometry) assume special significance in the crystal engineering of new materials.[14] Dan and Rao showed the progress of the conversion from a 0D to a 3D zinc-oxalato-piperazine framework by controlling the time and temperature of the hydrothermal synthesis.[15] The template effect of solvent molecules is also important, as described by Kwon et al. in the benzene-templated hydrotermal synthesis of the solvation compound $[Co_2(\mu\text{-ndc})_2(\mu\text{-bpe})]\cdot C_6H_6\cdot H_2O$ (ndc = 2,6-naphthalenedicarboxylate; bpe = 1, 2-bis(4-pyridyl)ethylene) or the triply interpenetrated $[Co_3(\mu\text{-ndc})_3(\mu\text{-bpe})1.5]\cdot H_2O$ structure, depending on whether benzene is present or not.[16] Within this area, we have focused our present work on the synthesis of new manganese−oxalato compounds with bpe in which the solution pH and the relative ratio of the reactants, thermal treatment, and the presence of different counterions play a key role in their final structures. The magnetic properties of the compounds are also investigated, and the magneto-structural correlations are discussed in detail.

Experimental Procedures

Syntheses. All chemicals were of reagent grade and were used as commercially obtained. $[Mn(\mu\text{-ox})(H_2O)_2]$ has been prepared according to the literature.[17]

$\{(Hbpe)_2[Mn_2(\mu\text{-ox})_3]\cdot\sim 0.8(C_2H_5OH)\cdot\sim 0.4(H_2O)\}_n$ (1). Single crystals of **1** were grown by layering an ethanolic solution of bpe (0.109 g, 0.6 mmol) and $Mn(NO_3)_2\cdot 4H_2O$ (0.050 g, 0.2 mmol) onto an aqueous solution of $H_2ox\cdot 2H_2O$ (0.038 g, 0.3 mmol). After allowing the solution to stand for two weeks, brown crystals were isolated using filtration. They were washed with cold water and diethyl ether and dried in the air. Yield: 85% (based on metal). Anal. Calcd for $C_{15.8}H_{13.8}MnN_2O_{6.6}$: C, 48.32; H, 3.52; N, 7.14; Mn, 14.00. Found: C, 48.42; H, 3.58; N, 7.13; Mn, 14.15%.

$\{[Mn(\mu\text{-ox})(\mu\text{-bpe})]\cdot xH_2O\}_n$ (2). Yellow single crystals of **2** were obtained by the slow diffusion of a methanol solution (20 mL) containing $Mn(NO_3)_2\cdot 4H_2O$ (0.075 g, 0.3 mmol) and bpe (0.055 g, 0.3 mmol) into an aqueous solution (10 mL) of $K_2ox\cdot H_2O$ (0.184 g, 1.0 mmol). They were washed with cold

(4) (a) Li, H.; Eddaoudi, M.; O'Keeffe, M.; Yaghi, O. M. *Nature* **1999**, *402*, 276. (b) Eddaoudi, M.; Kim, J.; Rosi, N.; Vodak, D.; Wachter, J.; O'Keeffe, M.; Yaghi, O. M. *Science* **2002**, *295*, 469. (c) Ma, B.-Q.; Mulfort, K. L.; Hupp, J. T. *Inorg. Chem.* **2005**, *44*, 4912. (d) Matsuda, R.; Kitaura, R.; Kitagawa, S.; Kubota, Y.; Belosludov, R. V.; Kobayashi, T. C.; Sakamoto, H.; Chiba, T.; Takata, M.; Kawazoe, Y.; Mita, Y. *Nature* **2005**, *436*, 238.

(5) (a) Seo, J. S.; Whang, D.; Lee, H.; Jun, S. I.; Oh, J.; Jeon, Y. J.; Kim, K. *Nature* **2000**, *404*, 982. (b) Mueller, U.; Schubert, M.; Teich, F.; Puetter, H.; Schierle-Arndt, K.; Pastré, J. *J. Mater. Chem.* **2006**, *16*, 626. (c) Mahata, P.; Madras, G.; Natarajan, S. *J. Phys. Chem.* **2006**, *110*, 13759. (d) Uemura, T.; Kitaura, R.; Ohta, Y.; Nagaoka, M.; Kitagawa, S. *Angew. Chem., Int. Ed.* **2006**, *45*, 4112.

(6) (a) Day, P. In *Supramolecular Engineering of Synthetic Metallic Materials*, Veciana, J., Rovira, C., Amabilino, D. B., Eds.; Kluwer Academic Publishers: New York, 1999; Nato Asi Series, Vol. *C518*, pp 253−269. (b) Verdaguer, M. *Polyhedron* **2001**, *20*, 1115. (c) Coronado, E.; Day, P. *Chem. Rev.* **2004**, *104*, 5419.

(7) (a) Atovmyan, L. O.; Shilov, G. V.; Lyubovskaya, R. N.; Ovanesyan, N. S.; Moronov, Y. G.; Pirumova, S. I.; Gusakovskaya, I. G. *JETP Lett.* **1993**, *58*, 818. (b) Carling, S. G.; Mathoniere, C.; Day, P.; Malik, K. M. A.; Coles, S. J.; Hursthouse, M. B. *J. Chem. Soc., Dalton Trans.* **1996**, 1839. (c) Coronado, E.; Galán-Mascarós, J. R.; Gómez-García, C. J.; Ensling, J.; Gütlich, P. *Chem.—Eur. J.* **2000**, *6*, 552. (d) Coronado, E.; Galán-Mascarós, J. R.; Goméz-García, C. J.; Laukhin, V. *Nature* **2000**, *408*, 447. (e) Martin, L.; Turner, S. S.; Day, P.; Guionneau, P.; Howard, J. A. K.; Hibbs, D. E.; Light, M. E.; Hursthouse, M. B.; Uruichi, M.; Yakushi, K. *Inorg. Chem.* **2001**, *40*, 1363. (f) Coronado, E.; Galán-Mascarós, J. R.; Gómez-García, C. J.; Martínez-Ferrero, E.; van Smaalen, S. *Inorg. Chem.* **2004**, *43*, 4808.

(8) (a) Decurtins, S.; Schmalle, H. W.; Schneuwly, P.; Oswald, H. R. *Inorg. Chem.* **1993**, *32*, 1888. (b) Decurtins, S.; Schmalle, H. W.; Pellaux, R.; Schneuwly, P.; Hauser, A. *Inorg. Chem.* **1996**, *35*, 1451. (c) Coronado, E.; Galán-Mascarós, J. R.; Gómez-García, C. J.; Martínez-Agudo, J. M. *Inorg. Chem.* **2001**, *40*, 113. (d) Andrés, R.; Brissard, M.; Gruselle, M.; Train, C.; Vaissermann, J.; Malézieux, B.; Jamet, J.-P.; Verdaguer, M. *Inorg. Chem.* **2001**, *40*, 4633. (e) Ballester, G.; Coronado, E.; Giménez-Saiz, C.; Romero, F. M. *Angew. Chem., Int. Ed.* **2001**, *40*, 792.

(9) (a) Román, P.; Guzmán-Miralles, C.; Luque, A.; Beitia, J. I.; Cano, J.; Lloret, F.; Julve, M.; Alvarez, S. *Inorg. Chem.* **1996**, *35*, 3741. (b) Cangussu, D.; Stumpf, H. O.; Adams, H.; Thomas, J. A.; Lloret, F.; Julve, M. *Inorg. Chim. Acta* **2005**, *358*, 2292. (c) Fuller, A. L.; Watkins, R. W.; Dunbar, K. R.; Prosvirin, A. V.; Arif, A. M.; Berreau, L. M. *Dalton Trans.* **2005**, 1891.

(10) (a) Castillo, O.; Luque, A.; Román, P.; Lloret, F.; Julve, M. *Inorg. Chem.* **2001**, *40*, 5526. (b) Castillo, O.; Luque, A.; Julve, M.; Lloret, F.; Román, P. *Inorg. Chim. Acta* **2001**, *315*, 9. (c) Castillo, O.; Luque, A.; Lloret, F.; Román, P. *Inorg. Chim. Acta* **2001**, *324*, 141.

(11) (a) García-Couceiro, U.; Castillo, O.; Luque, A.; García-Terán, J. P.; Beobide, G.; Román, P. *Eur. J. Inorg. Chem.* **2005**, 4280. (b) García-Couceiro, U.; Olea, D.; Castillo, O.; Luque, A.; Román, P.; de Pablo, P. J.; Gómez-Herrero, J.; Zamora, F. *Inorg. Chem.* **2005**, *44*, 8343.

(12) (a) García-Terán, J. P.; Castillo, O.; Luque, A.; García-Couceiro, U.; Román, P.; Lloret, F. *Inorg. Chem.* **2004**, *43*, 5761. (b) García-Terán, J. P.; Castillo, O.; Luque, A.; García-Couceiro, U.; Beobide, G.; Román, P. *Dalton Trans.* **2006**, 902.

(13) García-Couceiro, U.; Castillo, O.; Luque, A.; García-Terán, J. P.; Beobide, G.; Román, P. *Cryst. Growth Des.* **2006**, *6*, 1839.

(14) (a) Pan, L.; Frydel, T.; Sander, M. B.; Huang, X.; Li, J. *Inorg. Chem.* **2001**, *40*, 1271. (b) Laborda, S.; Clérac, R.; Anson, C. E.; Powell, A. K. *Inorg. Chem.* **2004**, *43*, 5931.

(15) (a) Dan, M.; Rao, C. N. R. *Angew. Chem., Int. Ed.* **2006**, *45*, 281. (b) Vaidhyanathan, R.; Natarajan, S.; Rao, C. N. R. *J. Chem. Soc., Dalton Trans.* **2001**, 699.

(16) Choi, E.-Y.; Park, K.; Yang, C.-M.; Kim, H.; Son, J.-H.; Lee, S. W.; Lee, Y. H.; Min, D.; Kwon, Y.-U. *Chem.—Eur. J.* **2004**, *10*, 5535.

(17) Kirschner, S. In *Inorganic Synthesis*; Rochow, E. G., Ed.; McGraw-Hill Book Co.: New York, 1960; Vol. *VI*.

water and diethyl ether and dried in the air. The anhydrous phase of compound **2** could be easily obtained as a yellow polycrystalline sample by adding the $K_2ox \cdot H_2O$ aqueous solution to the methanolic one. Yield: 90%. Anal. Calcd for $C_{14}H_{12}MnN_2O_5$ ($x = 1H_2O$): C, 49.00; H, 3.52; N, 8.16; Mn, 16.01. Found: C, 48.95; H, 3.57; N, 8.20; Mn, 16.03%.

$[Mn_2(\mu\text{-ox})_2(\mu\text{-bpe})(bpe)_2]_n$ (3). Compound **3** was synthesized as follows: 0.057 g (0.3 mmol) of $[Mn(\mu\text{-ox})(H_2O)_2]$ was dissolved in 30 mL of a hot water solution of $K_2ox \cdot H_2O$ (0.276 g, 1.5 mmol). Then, 15 mL of a methanolic solution containing bpe (0.164 g, 0.9 mmol) was added dropwise to the previous one. Immediately, a yellow polycrystalline powder of **2** appeared ($\sim$ 40%). After filtering off the precipitate, the resulting colorless solution was left to evaporate at room temperature. Yellow crystals of **3** appeared in a few days, and they were washed with cold water and diethyl ether and dried in the air. A polycrystalline sample of this compound was also obtained through the addition of an aqueous solution (10 mL) containing $K_2ox \cdot H_2O$ (0.055 g, 0.3 mmol) over an aqueous/methanolic solution (20 mL, 1/3 ratio) of $Mn(NO_3)_2 \cdot 4H_2O$ (0.075 g, 0.3 mmol) and bpe (0.164 g, 0.9 mmol). Yield: 80% Anal. Calcd for $C_{20}H_{15}MnN_3O_4$: C, 57.70; H, 3.63; N, 10.09; Mn, 13.20. Found: C, 57.63; H, 3.56; N, 10.12; Mn, 13.15%. The thermal treatment of compound **3** provides the new polymers **4a** and **4b**. The details of the solid state transformations are described in the structural description section.

$\{[Mn_4(\mu\text{-ox})_3(\mu\text{-bpe})_4(H_2O)_4] \cdot (X)_2 \cdot mY\}_n$ (X = NO_3^- for 5a, Br^- for 5b, and ClO_4^- for 5c; Y = solvation molecules). Complex **5a** was prepared by adding a methanolic solution (15 mL) of bpe (0.109 g, 0.6 mmol) dropwise to an aqueous solution (25 mL) that contained $Mn(NO_3)_2 \cdot 4H_2O$ (0.100 g, 0.4 mmol) and KNO_3 (0.243 g, 2.4 mmol). After that, 0.074 g of $K_2C_2O_4 \cdot H_2O$ (0.4 mmol) dissolved in 10 mL of water was added to the previous solution and was allowed to stir for 2 h. The resulting polycrystalline precipitate of compound **5a** was removed (yield 50−60%), and the colorless solution was left to evaporate at room temperature. Pale yellow crystals of the compound appeared in a few days, and they were washed with cold water and diethyl ether and dried in the air.

Complexes **5b** and **5c** were prepared by the same method, but using $MnBr_2 \cdot 4H_2O$ (0.115 g, 0.4 mmol), KBr (0.476 g, 4.0 mmol), bpe (0.109 g, 0.6 mmol), and $K_2C_2O_4 \cdot H_2O$ (0.074 g, 0.4 mmol) for **5b** and $Mn(ClO_4)_2$ (0.127 g, 0.5 mmol), $NaClO_4$ (0.489 g, 4.0 mmol), bpe (0.091 g, 0.5 mmol), and $K_2C_2O_4 \cdot H_2O$ (0.092 g, 0.5 mmol) for **5c**. After filtering off the initial precipitate, the resulting solution was left to evaporate at room temperature, and pale yellow crystals of **5b** and **5c** appeared in a few days. However, the crystals of compound **5c** were not of high enough quality to be analyzed by single crystal X-ray diffraction.

Anal. Calcd for $C_{54}H_{68}Mn_4N_{10}O_{32}$ (**5a**, Y = $10H_2O$): C, 40.82; H, 4.31; N, 8.82; Mn, 13.83. Found: C, 41.13; H, 4.02; N, 9.01; Mn, 13.52%. Anal. Calcd for $C_{58}H_{66}Br_2Mn_4N_8O_{17}$ (**5b**, Y = $5H_2O \cdot 4CH_3OH$): C, 41.81; H, 4.64; N, 6.61; Mn, 12.97. Found: C, 41.77; H, 4.47; N, 6.32; Mn, 13.01%. Anal. Calcd for $C_{66}H_{70}Cl_2Mn_4N_{10}O_{30}$ (**5c**, Y = $6H_2O \cdot$bpe): C, 44.69; H, 3.98; N, 7.90; Mn, 12.39. Found: C, 44.35; H, 3.85; N, 7.43; M_n 12.35%.

CAUTION! *Perchlorate salts of metal complexes with organic ligands are potentially explosive and should be handled with care.*

Physical Measurements. Elemental analyses (C, H, N) were performed on a Perkin-Elmer 2400 microanalytical analyzer. The metal content was determined by absorption spectrometry. The purity and homogeneity of the polycrystalline samples used for physical measurements were checked using IR spectroscopy, elemental analysis, and X-ray powder diffraction methods. The IR spectra (KBr pellets) were recorded on a FTIR Mattson 1000 spectrometer in the 4000−400 cm^{-1} spectral region. Magnetic measurements were performed on polycrystalline samples of the complexes taken from the same uniform batches used for the structural determinations with a Quantum Design SQUID susceptometer covering the temperature range 5.0−300 K at a magnetic field of 1000 G. The susceptibility data were corrected for the diamagnetism estimated from Pascal's tables,[18] the temperature-independent paramagnetism, and the magnetization of the sample holder. Thermal analyses (TG/DTA) were performed on a TA Instruments SDT 2960 thermal analyzer in a synthetic air atmosphere (79% N_2/21% O_2) with a heating rate of 5 °C min^{-1}.

X-Ray Diffraction Data Collection and Structure Determination. Diffraction data of single crystals of **1**−**3**, **5a**, and **5b** were collected at 293(2) K on an Oxford Diffraction Xcalibur diffractometer with graphite-monochromated Mo Kα radiation (λ = 0.71073 Å). The data reduction was done with the CrysAlis RED program.[19] All structures were solved with direct methods using the SIR92 program[20] and refined using full-matrix least-squares on F^2, including all reflections (SHELXL93).[21] All calculations were performed using the WINGX crystallographic software package.[22] After completing the initial structure solution, the difference Fourier map for compounds **5a** and **5b** showed the presence of substantial electron density at the channels of the structures, and it could not be possible to find a model for the guest molecules. The contribution of these molecules was subtracted from the reflection data by the SQUEEZE method[23] as implemented in PLATON.[24] An estimation of the proportion of guest molecules was obtained from the TG/DTA curves (see the Supporting Information) and elemental analyses. The final geometrical calculations and the graphical manipulations were carried out with the PARST95[25] and PLATON[24] programs. During the data reduction process, it becomes clear that the crystal specimens of compound **5b** were twinned; therefore, the *hkl* file corresponding to the major domain of the nonmerohedral twin was processed to avoid reflections with significant contributions from the minor domains.[26] Details of the structure determination and refinement of the compounds are summarized in Table 1. Crystallographic data (excluding structure factors) for the structures reported in this paper have been deposited with the Cambridge Crystallographic Data Center as supplementary publication nos. CCDC 776261−776265. Copies of the data can be obtained free of charge on application to the Director, CCDC, 12 Union Road, Cambridge, CB2 1EZ, U. K. (fax: +44−1223−335033; e-mail: deposit@ccdc.cam.ac.uk; or http://www.ccdc.cam.ac.uk).

The X-ray powder diffraction (XRPD) pattern for compound **5c** was collected on a Phillips X'PERT powder diffractometer with Cu Kα radiation (λ = 1.5418 Å) over the range $5 < 2\theta < 40°$ with a step size of 0.02° and an acquisition time of 4 s per step at 25 °C. Indexation of the diffraction profiles was made by means of the FULLPROF program (pattern-matching analysis)[27] on the basis of the space group and the cell parameters found for compound **5a** by single crystal X-ray diffraction. The unit cell parameters obtained in the final refinement were a = 13.899(1) Å, b = 11.444(1) Å, c = 24.860(2) Å, and β = 90.32(1)°. The

(18) Earnshaw, A. *Introduction to Magnetochemistry*; Academic Press: London, 1968.
(19) *CrysAlis RED*, version 1.170; Oxford Diffraction: Wroclaw, Poland, 2003.
(20) Altomare, A.; Cascarano, M.; Giacovazzo, C.; Guagliardi, A. *J. Appl. Crystallogr.* **1993**, *26*, 343.
(21) Sheldrick, G. M. *SHELXL93*; Universitat of Göttingen: Göttingen, Germany, 1993.
(22) Farrugia, L. J. *WINGX*; University of Glasgow: Glasgow, Great Britain, 1998.
(23) Van der Sluis, P.; Spek, A. L. *Acta Crystallogr.* **1990**, *A46*, 194.
(24) Spek, A. L. *Acta Crystallogr.* **1990**, *A46*, C34.
(25) Nardelli, M. *J. Appl. Crystallogr.* **1995**, *28*, 659.
(26) Bolte, M. *J. Appl. Crystallogr.* **2004**, *37*, 162.
(27) (a) Rodríguez-Carvajal, J. *FULLPROF, Program Rietveld for Pattern Matching Analysis of Powder Patterns*, Abstracts of the Satellite Meeting on Powder Diffraction of the XV Congress of the IUCr, Toulouse, France, 1990; p 127. (b) Rodríguez-Carvajal, J. *FULLPROF 2000*, version 2.5d; Laboratoire Léon Brillouin (CEA-CNRS), Centre d'Études de Saclay: Gif sur Yvette Cedex, France, 2003.

Table 1. Single-Crystal Data and Structure Refinement Details of compounds **1**−**3**, **5a**, and **5b**

	1	**2**	**3**	**5a**	**5b**
empirical formula	$C_{15.8}H_{13.8}MnN_2O_{6.6}$	$C_{14}H_{12}MnN_2O_5$	$C_{20}H_{15}MnN_3O_4$	$C_{27}H_{24}Mn_2N_5O_{11}$	$C_{27}H_{24}BrMn_2N_4O_8$
fw	392.35	343.18	416.29	704.39	722.29
cryst syst	triclinic	triclinic	monoclinic	monoclinic	monoclinic
space group	$P\bar{1}$	$P\bar{1}$	$P2_1/n$	$P2_1/c$	$P2_1/c$
a (Å)	9.289(3)	9.243(1)	9.539(2)	13.748(2)	13.872(5)
b (Å)	9.538(2)	9.727(1)	11.024(2)	11.343(1)	11.443(2)
c (Å)	10.335(3)	9.732(1)	16.925(4)	24.652(2)	24.711(3)
α (deg)	81.03(2)	106.00(1)	90	90	90
β (deg)	84.26(2)	116.48(1)	106.38(2)	92.98(1)	93.27(2)
γ (deg)	66.16(2)	90.66(1)	90	90	90
V (Å^3)	826.6(4)	743.6(1)	1707.6(6)	3839.1(7)	3916(2)
Z	2	2	4	4	4
ρ_{calc} (g cm^{-3})	1.565	1.472	1.619	1.219	1.225
μ (mm^{-1})	0.838	0.907	0.808	0.711	1.706
F(000)	395.3	339	852	1436	1452
reflns collected	7244	7422	13401	37861	29169
independent reflns	3962	4273	4118	11168	9459
GOF	0.827	0.957	0.806	0.999	0.827
R_{int}	0.0422	0.0372	0.0952	0.0735	0.1579
final R indices [$I > 2\sigma(I)$] R1[a]/wR2[a]	0.0506/0.1048	0.0439/0.1008	0.0495/0.0758	0.062/0.1788	0.0852/0.2296
all data R1[a]/wR2[a]	0.1116/0.1167	0.0601/0.1041	0.2240/0.1212	0.1151/0.1867	0.1711/0.2718

[a] $R1 = \sum(|F_o| - |F_c|)/\sum|F_o|$. $wR2 = [\sum w(F_o^2 - F_c^2)^2/\sum w(F_o^2)^2]^{1/2}$; $w = 1/[\sigma^2(F_o^2) + (AP)^2]$ with $P = (|F_o|^2 + 2|F_c|^2)/3$. $A = 0.0454$ for **1**, 0.0588 for **2**, 0.0168 for **3**, 0.0877 for **5a**, 0.1549 for **5b**.

calculated and observed diffraction patterns are shown in the Supporting Information. The presence of some small unaccounted for Bragg peaks in the diffraction pattern has been attributed to the presence of a small amount of impurity.

Variable-temperature X-ray powder diffraction measurements of compound **3** were run under an ambient atmosphere in the range $8 < 2\theta < 38°$ with a step size of 0.03° and an acquisition time of 2 s per step. The compound was heated up to 65 °C with a heating rate of 10 °C min^{-1}, and after that, diagrams were collected every 15 °C with a heating rate of 5 °C min^{-1} up to 470 °C. The indexation of the diffraction patterns of compounds **4a** and **4b** obtained from the thermal treatment of compound **3** gives rise to the following cell parameters: a = 5.311(2) Å, b = 8.514(2) Å, c = 9.224(5) Å, α = 109.96(3)°, β = 94.13(2)°, and γ = 97.14(4)° for compound **4a** and a = 5.832(5) Å, b = 7.872(5) Å, c = 8.854(5) Å, α = 113.68(2)°, β = 90.49(3)°, and γ = 107.20(7)° for compound **4b**. The calculated and observed diffraction patterns are shown in the Supporting Information.

Results and Discussion

Synthesis of the Mn(II)/Oxalate/bpe System. As we will describe in the article, we were able to obtain a wide variety of crystal structures based on the same system, Mn(II)/oxalate/bpe, by controlling the synthetic conditions (Scheme 1). In acid media, the bpe ligand is monoprotonated, and it acts as a template during the crystallization process and allows the formation of the anionic 2D honeycomb $[Mn_2(\mu\text{-ox})_3]_n^{2-}$ framework (**1**). At neutral or basic pH, two neutral compounds build up in the reaction solution depending on the relative Mn/bpe ratio. The three-dimensional compound **2** with formula [Mn(ox)(bpe)] is grown in an equimolecular mixture of the reactants [$Mn(NO_3)_2$/bpe/$K_2C_2O_4$]. The increase of the Mn/bpe ratio of the reaction leads to complex **3**, composed of $[Mn_2(ox)_2(bpe)_3]$ sheets. The two different crystal structures also imply a change in the metal−oxalato skeleton, which varies from zigzag chains with *cis*-coordinated bpe ligands in compound **2** to a linear one in which the bpe molecules are *trans*-coordinated.

It is worth highlighting that the slow diffusion of the reagents in the synthesis of compound **2** produces the hydrated form, while the direct reaction leads to the anhydrous phase. This fact seems to indicate that the slow crystal growth process permits water molecules to move into the 3D network up to where they were occluded, while if the structure is built up very fast, the compact framework prevents the hydration. It is possible to obtain different hydration rates according to the crystal growth speed, which would explain the different occupancy factors of the water molecules found in compound **2**.

Finally, we also observed that the presence of an excess of counterions in the reaction media acted as a template in the crystallization of the open framework structure **5**. This compound can be synthesized with bromide, nitrate, or perchlorate, and a partial substitution of the anions for chloride was realized, although it could not be directly synthesized. The use of more voluminous ions such as BF_4^- or PF_6^- did not direct the growth toward any crystalline phase containing these ions, which implies that the size of the counterion acting as a template is a crucial factor in the crystallization process of compound **5**.

Crystal Structure of $\{(Hbpe)_2[Mn_2(\mu\text{-ox})_3]\cdot\sim 0.8(C_2H_5OH)\cdot\sim 0.4(H_2O)\}_n$ (1). The crystal structure of compound **1** consists of stacked $[Mn_2(\mu\text{-ox})_3]^{2-}$ layers with cationic $Hbpe^+$ molecules intercalated between them. Manganese(II) metal centers are coordinated to three independent centrosymmetric bis-bidentate oxalato ligands, yielding a slightly distorted octahedral O_6 donor set. A view of the coordination sphere of the metal center and cationic bpe molecules is shown in Figure 1, and selected bond distances and angles are listed in Table 2. The Mn−O bond distances and the separation of the manganese atoms along the oxalato bridge (5.583, 5.617, and 5.655 Å) are in the range observed for other manganese−oxalato compounds.[11b,28] The oxalato ligands link the Mn(II) atoms to form anionic honeycomb layers of alternative Δ- and Λ-$[Mn_2(\mu\text{-ox})_3]^{2-}$ units with a distance between layers of 10.22 Å. These sheets are piled up, creating hexagonal channels along the c axis

(28) (a) Glerup, J.; Goodson, P. A.; Hodgson, D. J.; Michelsen, K. *Inorg. Chem.* **1995**, *34*, 6255. (b) Fuller, A. L.; Watkins, R. W.; Dunbar, K. R.; Prosvirin, A. V.; Arif, A. M.; Berreau, L. M. *Dalton Trans.* **2005**, 1891.

Scheme 1.[a]

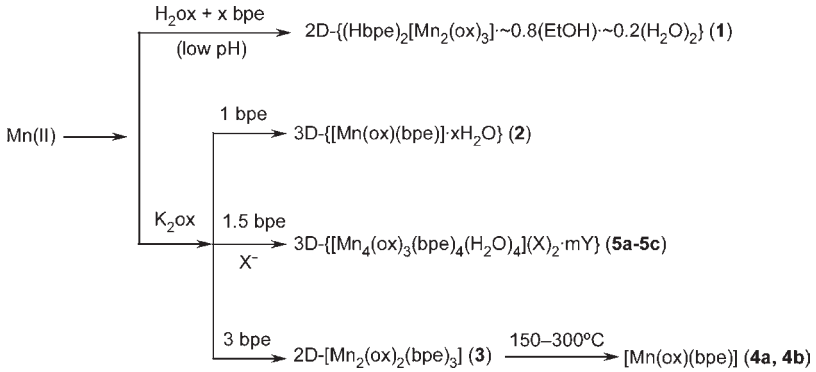

[a] X = NO_3^- (**5a**), Br^- (**5b**), ClO_4^- (**5c**); Y = solvation molecules.

(Figure 2a). However, $Hbpe^+$ molecules form a rigid cationic network intercalated between the anionic layers, occluding the channels and giving rise to hexagonal cavities with a free volume per unit formula of 120.8 Å^3 (14.6%). The cavities contain disordered ethanol and water molecules, forming a two-dimensional host−guest system.

The cationic network is constructed of two crystallographically independent monoprotonated bpe molecules which are joined together by N−H···N hydrogen bonds to form chains running along the [120] direction. In addition, the midpoint of the ethylene bond of one molecule faces the center of the pyridine ring of the adjacent molecule linking the chains by *face-to-face* $\pi-\pi$ interactions (see the Supporting Information) to form a rigid two-dimensional net (Figure 2b). The close related compound $\{(DAPS)[MnCr(\mu\text{-ox})_3]\cdot CH_3CN\}_n$[29] (DAPS = 4-[4-(dimethylamino)-α-styryl]-N-methylpyridinium) presents a similar cationic $\pi-\pi$ packing between a C=C bond and the pyridine ring in the DAPS molecules, leading to supramolecular linear aggregates.

The mean planes of bpe molecules are nearly perpendicular to the manganese−oxalato anionic layers (Figure 2c). bpe1 was found to be disordered in two positions twisted with each other at 14.1° and could be refined isotropically with 78%/22% occupancy factors. The ethylene bond of bpe2 is placed between two oxalato ligands of consecutive layers forming C−H···O_{ox} hydrogen bonds. The supramolecular three-dimensional structure of the titled compound is built up by means of an extensive net of hydrogen bonds which assembles the layers along the *c* axis (see the Supporting Information). A view of the three-dimensional crystal packing of compound **1** is shown in Figure 2d.

The robustness of the crystal building is confirmed by its high thermal stability (see the Supporting Information). The thermogravimetric analysis shows that under a synthetic air atmosphere, compound **1** retains its structure up to 300 °C, after which a very exothermic process takes place to give Mn_2O_3 above 360 °C, with a total weight loss of 80.7% (calcd 79.9%). The TG curve does not show any loss of weight before the degradation process, which implies that the guest molecules are occluded in the metal−oxalato framework.

Crystal Structure of $\{[Mn(\mu\text{-ox})(\mu\text{-bpe})]\cdot xH_2O\}_n$ (2). The crystal structure of compound **2** consists of zigzag Mn(II)−oxalato chains joined between them by *cis*-coordinated bpe ligands forming a three-dimensional network. The asymmetric unit is comprised by one metal center, two centrosymmetric oxalate dianions, two centrosymmetric bpe ligands, and a water solvation molecule (Figure 3). Selected bond distances and angles are reported in Table 3. The metal centers are joined by bis-bidentate oxalate dianions (M···M = 5.681 and 5.684 Å) forming a zigzag chain, with a dihedral angle of 85.5° between them. The pyridine molecules coordinated to the Mn(II) atoms are twisted 53.1° between them, establishing within the sheet C−H···π interactions (H···Cent, 3.15 Å; C−H···Cent, 133.6°; C···Cent, 3.85 Å, where Cent is the centroid of the pyridine ring) between C26 and the aromatic ring of the other molecule.[30] Each chain is joined to the other four by bis-monodentate bpe ligands, building up an open three-dimensional network with channels of approximate dimensions of 24 × 16 Å running along the *b* axis (Figure 4). However, three networks are interpenetrated, giving rise to a compact 3D framework that reduces drastically the size of the channels. The topological analysis carried out by means of the TOPOS program package[31] indicates a three interpenetrating diamond like 3D network (4-c net), the Schlaffli symbol being (6^6).

Each interpenetrated 3D network is involved in an extended system of C−H···O_{ox} hydrogen bonds established between bpe molecules and the oxalato oxygen atoms belonging to adjacent 3D frameworks (see the Supporting Information). The crystallization water molecule was occluded in the structure, and its occupancy factor was refined up to 25%. The position of the hydrogen atoms of the water molecule was calculated using Nardelli's method.[32] The occluded water molecule establishes two hydrogen bonds, with an oxalate oxygen atom and with the aromatic pyridine ring of a bpe molecule from a neighboring 3D network.

(29) Bérnard, S.; Yu, P.; Audière, J. P.; Rivière, E.; Clément, R.; Guilhem, J.; Tchertanov, L.; Nakatani, K. *J. Am. Chem. Soc.* **2000**, *122*, 9444.

(30) (a) Abu-Youssef, M. A. M.; Escuer, A.; Goher, M. A. S.; Mautner, F. A.; Reib, G. J.; Vicente, R. *Angew. Chem., Int. Ed.* **2000**, *39*, 1624. (b) Abu-Youssef, M. A. M.; Drillon, M.; Escuer, A.; Goher, M. A. S.; Mautner, F. A.; Vicente, R. *Inorg. Chem.* **2000**, *39*, 5022. (c) Ghosh, A. K.; Ghoshal, D.; Zangrando, E.; Ribas, J.; Chaudhuri, N. R. *Inorg. Chem.* **2005**, *44*, 1786.

(31) TOPOS Main Page. http://www.topos.ssu.samara.ru (accessed Nov 2010). Blatov, V. A. *IUCr CompComm. Newslett.* **2006**.

(32) Nardelli, M. *J. Appl. Crystallogr.* **1999**, *32*, 563.

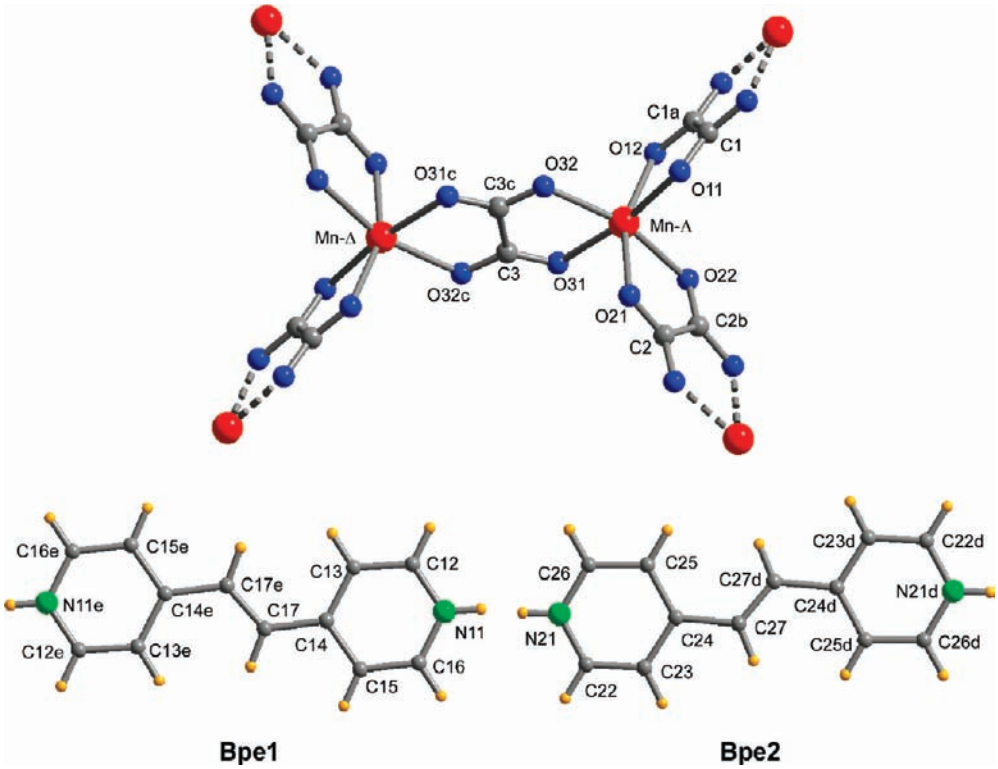

Figure 1. View of the Mn(II) coordination sphere and the two crystallographically independent cationic bpe molecules in compound **1**. Only the major component of bpe with a population of 78% is shown (bpe1). Symmetry codes: (a) $1-x, -y, -z$; (b) $1-x, 1-y, -z$; (c) $-x, 1-y, -z$; (d) $2-x, 1-y, 1-z$; (e) $-x, -y, 1-z$.

Table 2. Selected Bond Lengths (Å) and Angles (deg) of $\{(Hbpe)_2[Mn_2(\mu\text{-}ox)_3]\cdot\sim 0.8(C_2H_5OH)\cdot\sim 0.4(H_2O)\}_n$ (**1**)

Mn−O(11)	2.189(3)	Mn−O(12)	2.160(3)
Mn−O(21)	2.158(2)	Mn−O(22)	2.175(2)
Mn−O(31)	2.165(2)	Mn−O(32)	2.189(2)
O(11)−Mn−O(12)	76.04(9)	O(12)−Mn−O(32)	102.86(10)
O(11)−Mn−O(21)	89.24(10)	O(21)−Mn−O(22)	76.98(9)
O(11)−Mn−O(22)	95.46(10)	O(21)−Mn−O(31)	99.16(10)
O(11)−Mn−O(31)	171.13(9)	O(21)−Mn−O(32)	87.29(10)
O(11)−Mn−O(32)	100.43(10)	O(22)−Mn−O(31)	89.25(10)
O(12)−Mn−O(21)	163.33(10)	O(22)−Mn−O(32)	157.46(9)
O(12)−Mn−O(22)	96.40(10)	O(31)−Mn−O(32)	77.29(9)
O(12)−Mn−O(31)	96.01(10)		

The thermogravimetric measurements of compound **2** performed over samples obtained from the diffusion test tube show a first exothermic process that starts at 175 °C, and it is completed around 220 °C and corresponds to the release of one water molecule (DTA peak, 190 °C; weight loss, exp., 5.80%, calcd, 5.25%). The anhydrous phase is stable up to 300 °C, after which an exothermic process takes place to give Mn_2O_3 as the final product above 370 °C (DTA peak, 345 °C; weight loss, exp., 76.45%, calcd, 77.00%). These data are in good agreement with the elemental analysis performed on the overall sample of compound **2**, which implies one water molecule per formula unit. Nonetheless, the X-ray crystal analysis provides only 25% of the water in the 3D framework. The fact that the loss of the water molecule was an exothermic process implies that the dense 3D interpenetrated structure occludes it, preventing an easy displacement of the water molecule, which is confirmed by the high temperature of the dehydration process. It also seems to indicate that the hydration of the compound could not be a diffusion process, and it takes place during the crystal growth. Our attempts to rehydrate the anhydrous compound were unsuccessful, confirming that water molecules are unable to diffuse along the crystal structure. Finally, we were able to isolate different degrees of hydration controlling the crystallization time.

Crystal Structure of $[Mn_2(\mu\text{-ox})_2(\mu\text{-bpe})(bpe)_2]_n$ (3). Compound **3** crystallizes in the monoclinic space group $P2_1/n$. Its structure consists of manganese(II) metal centers coordinated by bis-bidentate oxalato ligands to form corrugated one-dimensional chains running along the *b* direction which are cross-linked by bis-monodentated bpe molecules to result in neutral two-dimensional sheets spreading along the (103) plane. The metal center is coordinated to four oxygen atoms from two oxalate anions and two nitrogen atoms from the bpe molecules to form a distorted octahedral O_4N_2 environment (Figure 5). Selected bond lengths and angles are gathered in Table 4. The two oxalato groups around the Mn atom are twisted 18.7°, leading a corrugated metal−oxalato chain with a Mn···Mn···Mn angle of 168.7° and a distance through the oxalato bridges of 5.539 Å.

The metal atom is coordinated by two different bpe molecules which serve as either a terminal or a bridging ligand with an angle of 46° between them, giving rise to a broken ladder-like 2D polymer. The centrosymmetric bridging bpe ligand generates the layers by joining the metal−oxalato chains with a Mn···Mn distance of 13.91 Å (Figure 6). The remaining bpe molecule is terminally coordinated and was found to be disordered in two positions twisted by 2.5°. In both cases, the molecule is near planar with a dihedral angle between the pyridine rings of 7.3°

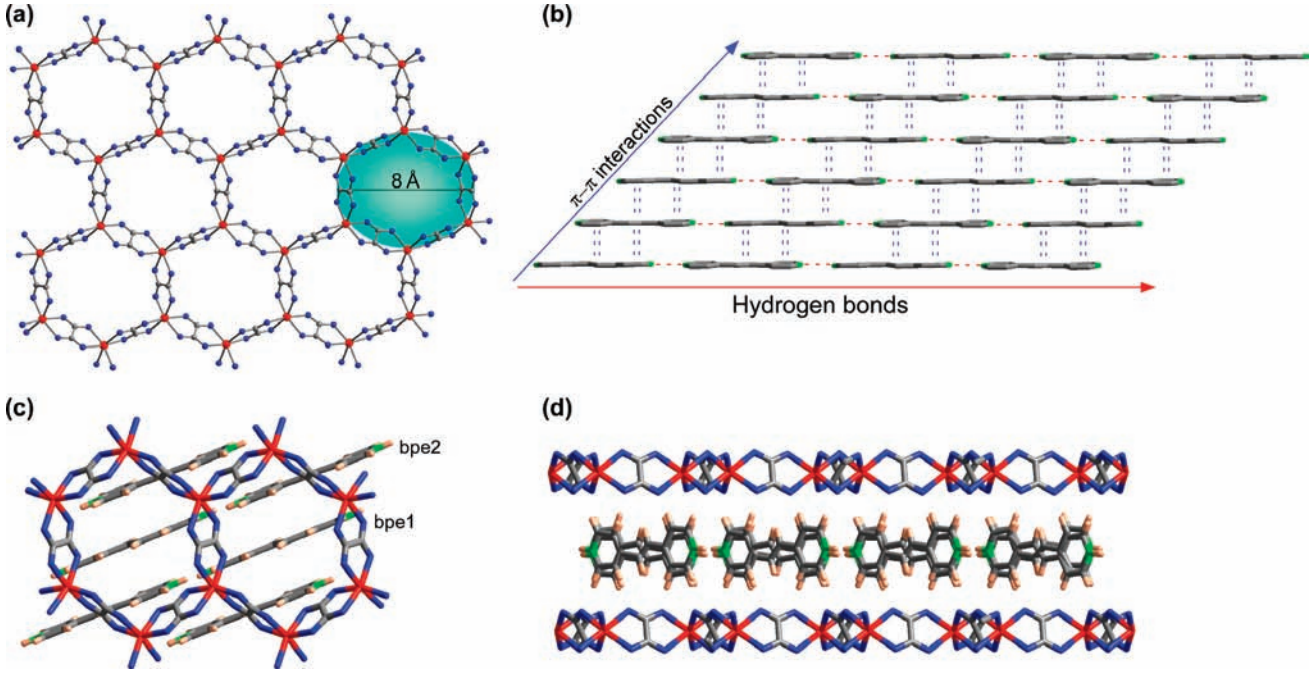

Figure 2. (a) Representation of the honeycomb $[Mn_2(\mu\text{-ox})_3]_n^{2-}$ layers of compound **1**. (b) Packing of the cationic molecules. (c) Location of the $Hbpe^+$ molecules in the framework. (d) View of the 3D crystal structure in the *ac* plane.

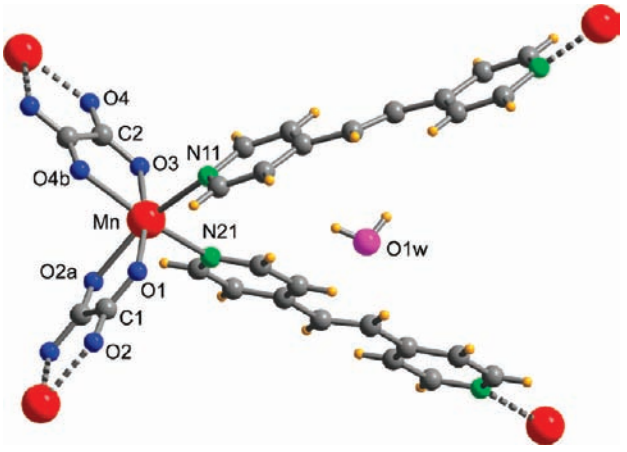

Figure 3. View of the Mn(II) coordination sphere of compound **2**. Symmetry codes: (a) $-x, -y, -z$; (b) $-x, 1-y, -z$.

(for the major occupancy) and 8.5° (for the minor occupancy). 1,2-Bis(4-pyridyl)ethylene ligand exhibits an almost coplanar conformation in the great majority of its complexes, although rare examples have been reported with dihedral angles up to 74°.[33] As is shown in Figure 6, there are two terminal bpe molecules between the bridging ones, and they are near planar between them, which allows the presence of *face-to-face* intralayer $\pi-\pi$ contacts (see the Supporting Information). The polymeric metal–organic sheets are stacked by weak C–H···O hydrogen bonds involving the aromatic pyridine rings, the ethylene hydrogen atoms, and the oxalato bridging ligand, which leads to the overall three-dimensional supramolecular architecture with an interlayer distance of 5.37 Å (see the Supporting Information).

Table 3. Selected Bond Lengths (Å) and Angles (deg) of $[Mn(\mu\text{-ox})(\mu\text{-bpe})]_n$ (**2**)[a]

Mn–O(1)	2.166(1)	Mn–O(3)	2.186(1)
Mn–O(2)a	2.210(1)	Mn–O(4)b	2.182(1)
Mn–N(11)	2.274(2)	Mn–N(21)	2.296(2)
O(1)–Mn–O(2)a	76.02(5)	O(2)a–Mn–N(21)	87.35(6)
O(1)–Mn–O(3)	169.54(5)	O(3)–Mn–O(4)b	75.63(5)
O(1)–Mn–O(4)b	95.73(6)	O(3)–Mn–N(11)	99.24(6)
O(1)–Mn–N(11)	87.65(6)	O(3)–Mn–N(21)	83.24(6)
O(1)–Mn–N(21)	104.75(6)	O(4)b–Mn–N(11)	97.79(7)
O(2)a–Mn–O(3)	97.95(6)	O(4)b–Mn–N(21)	158.39(6)
O(2)a–Mn–O(4)b	91.06(6)	N(11)–Mn–N(21)	89.95(6)
O(2)a–Mn–N(11)	162.15(6)		

[a] Symmetry codes: (a) $-x, -y, -z$; (b) $-x, 1-y, -z$.

It is worth pointing out that the orientation of the terminal bpe molecules with respect to the adjacent metal–oxalato framework locates the noncoordinated nitrogen atom just above the carbon–carbon bond of the oxalato ligand. The N···C distances range from 2.85 Å to 2.91 Å, and the dihedral angle between the pyridine ring and the mean plane of the oxalato anion is of about 85°. The same perpendicular arrangement of the oxalato ligand and N-containing aromatic rings has been previously observed by our group in a family of metal–oxalato one-dimensional compounds with purine (pur).[12] The crystal structure of these compounds of general formula $[M(\mu\text{-ox})(H_2O)(pur)]$ (M(II) = Mn, Co, Cu and Zn) consists of one-dimensional zigzag chains in which the purine molecule coordinated to the metal center is parallel to the propagation direction of the chain. The nonprotonated pyrimidinic N3 atom is located over the carbon–carbon bond of the oxalato ligand with a mean distance of 3.0 Å and a dihedral angle between the two ligands of about 90°. This fact precludes the involvement of the potential hydrogen-bonding N3 atom in any other interaction. Although not cited, this arrangement could

(33) (a) Zakaria, C. M.; Ferguson, G.; Lough, A. J.; Glidewell, C. *Acta Crystallogr., Sect. C* **2002**, *58*, m1. (b) Li, X.; Cao, R.; Sun, D.; Bi, W.; Wang, Y.; Li, X.; Hong, M. *Cryst. Growth Des.* **2004**, *4*, 775. (c) Lai, C. S.; Tiekink, E. R. T. *CrystEngComm* **2004**, *6*, 593. (d) Jayaraman, A.; Balasubramaniam, V.; Valiyaveettil, S. *Cryst. Growth Des.* **2006**, *6*, 636.

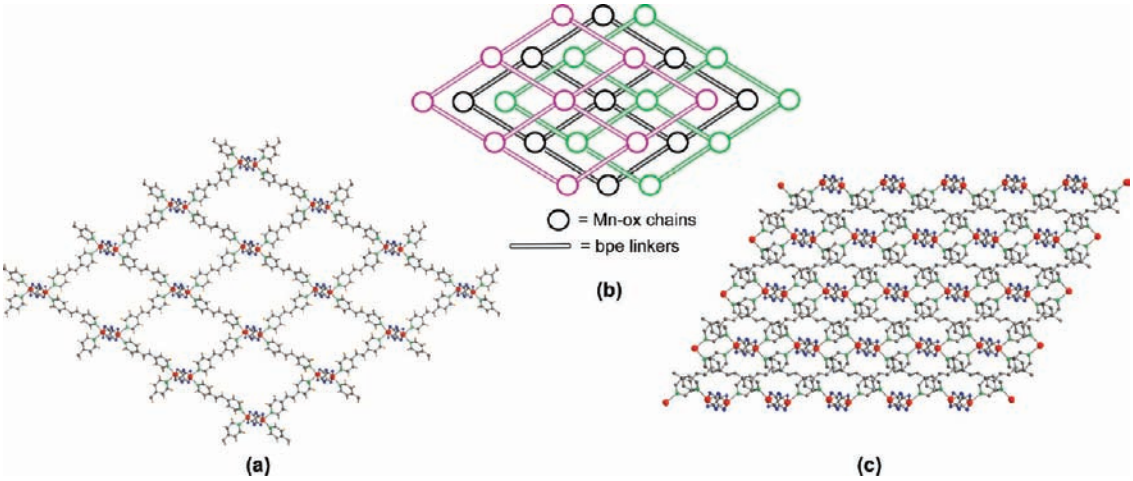

Figure 4. (a) View of the 3D network of compound **2** along the growing Mn−ox chains (*b* axis), showing the channels. (b) Schematic representation of the triple interpetration. (c) View of the 3D framework along the *b* axis.

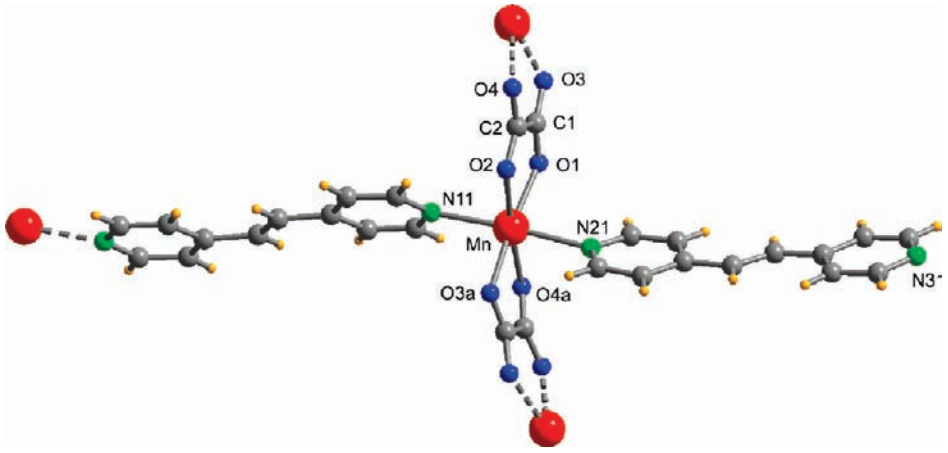

Figure 5. View of the Mn(II) coordination sphere of compound **3**. Only the major component of terminal bpe with a population of 69% is shown. Symmetry code: (a) $3/2 - x$, $1/2 + y$, $1/2 - z$.

Table 4. Selected Bond Lengths (Å) and Angles (deg) of $[Mn_2(\mu\text{-ox})_2(\mu\text{-bpe})(bpe)_2]_n$ (**3**)[a]

Mn−O(1)	2.165(4)	Mn−O(3)a	2.183(4)
Mn−O(2)	2.169(4)	Mn−O(4)a	2.180(4)
Mn−N(11)	2.306(5)	Mn−N(21)	2.313(12)
		Mn−N(21B)	2.33(3)
O(1)−Mn−O(2)	77.1(1)	O(2)−Mn−N(21)	93.1(3)
O(1)−Mn−O(3)a	174.6(1)	O(2)−Mn−N(21B)	89.1(7)
O(1)−Mn−O(4)a	102.9(1)	O(3)a−Mn−N(11)	93.2(1)
O(2)−Mn−O(3)a	102.3(1)	O(3)a−Mn−N(21)	84.9(3)
O(2)−Mn−O(4)a	175.5(1)	O(3)a−Mn−N(21B)	80.2(5)
O(3)a−Mn−O(4)a	77.2(1)	O(4)a−Mn−N(11)	93.5(1)
O(1)−Mn−N(11)	92.2(2)	O(4)a−Mn−N(21)	82.5(3)
O(1)−Mn−N(21)	93.1(3)	O(4)a−Mn−N(21B)	86.5(7)
O(1)−Mn−N(21B)	94.4(5)	N(11)−Mn−N(21)	175.8(3)
O(2)−Mn−N(11)	91.0(2)	N(11)−Mn−N(21B)	173.2(5)

[a] Symmetry code: (a) $3/2 - x$, $1/2 + y$, $1/2 - z$.

also be observed in the closely related bidimensional compounds $[M_3(\mu\text{-ox})_3(4bpy)_4]$ (M(II) = Mn, Fe, Cu, Zn; 4bpy = 4,4′-bipyridine)[34] and $[Cu_2(\mu\text{-ox})_2(pyz)_3]$ (pyz = pyrazine),[35] which are built up by metal−oxalato chains joined by 4bpy or pyz ligands.

The thermal analysis of compound **3** shows a first weight loss between 165 and 215 °C (exptl, 20.1%; calcd, 21.9%) that provides crystalline compound **4**, which remains stable up to 300 °C. Then, it undergoes one very exothermic process to lead Mn_2O_3 above 380 °C. The variable-temperature X-ray powder diffraction measurements (Figure 7) agree with the thermal analysis. The XRPD profile at 65 °C matches the simulated pattern generated from the crystal structure of **3**, and no change is observed up to 155 °C, when the diffraction diagram changes to provide a new crystalline phase **4a** (the elemental analysis of compound **4a** agrees with the molecular formula [Mn(ox)(bpe)]; Anal. Calcd for $C_{14}H_{10}MnN_2O_4$: C, 51.71; H, 3.10; N, 8.61; Mn, 16.89. Found: C, 51.15; H, 2.95; N, 8.35; Mn, 16.93%). The XRPD patterns remain unaltered up to 290 °C, after which a decrease in the crystallinity was observed, leading to an amorphous phase. Finally, when a temperature of 365 °C is reached, peaks of Mn_2O_3 appear.

To provide a deeper insight into the thermally obtained compound **4a**, the starting compound **3** was heated from

(34) (a) Zheng, L.-M.; Fang, X.; Lii, K.-H.; Song, H.-H.; Xin, X.-Q.; Fun, H.-K.; Chinnakali, K.; Razak, I. A. *J. Chem. Soc., Dalton Trans.* **1999**, 2311. (b) Castillo, O.; Alonso, J.; García-Couceiro, U.; Luque, A.; Román, P. *Inorg. Chem. Commun.* **2003**, *6*, 803. (c) Nordell, K. J.; Higgins, K. A.; Smith, M. D. *Acta Crystallogr.* **2003**, *E59*, m114. (d) Zhu, L.-H.; Zeng, M.-H.; Ng, S. W. *Acta Crystallogr.* **2005**, *E61*, m916.

(35) Kitagawa, S.; Okubo, T.; Kawata, S.; Kondo, M.; Katada, M.; Kobayasi, H. *Inorg. Chem.* **1995**, *34*, 4790.

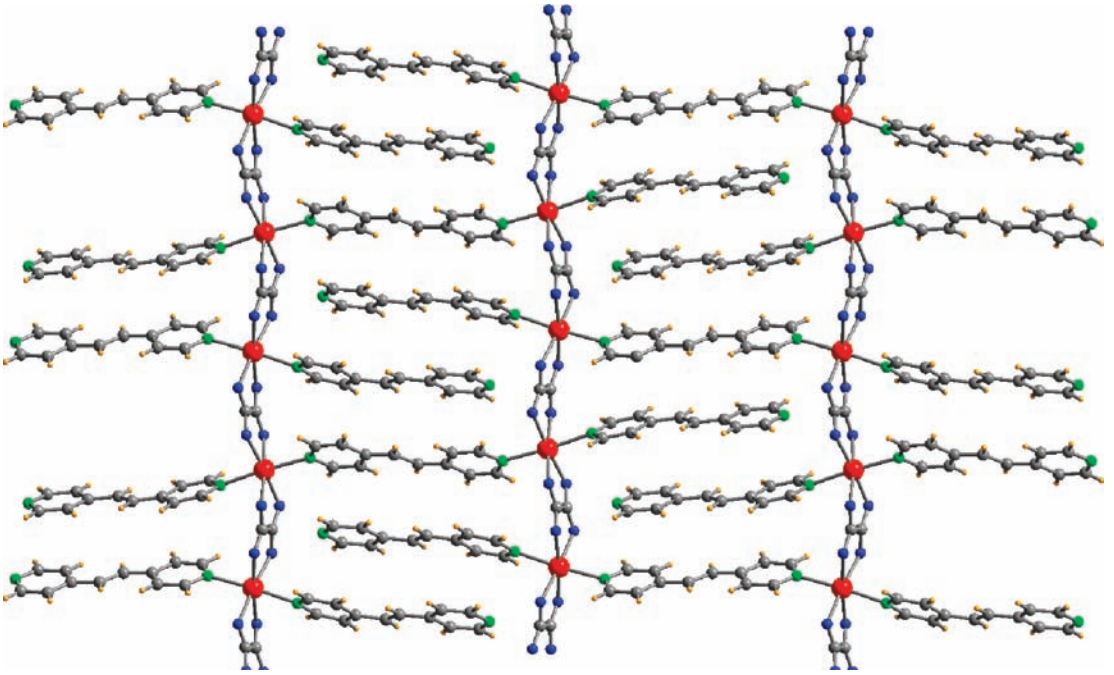

Figure 6. One layer of the broken ladder-like structure of compound **3** viewed along the [103] direction.

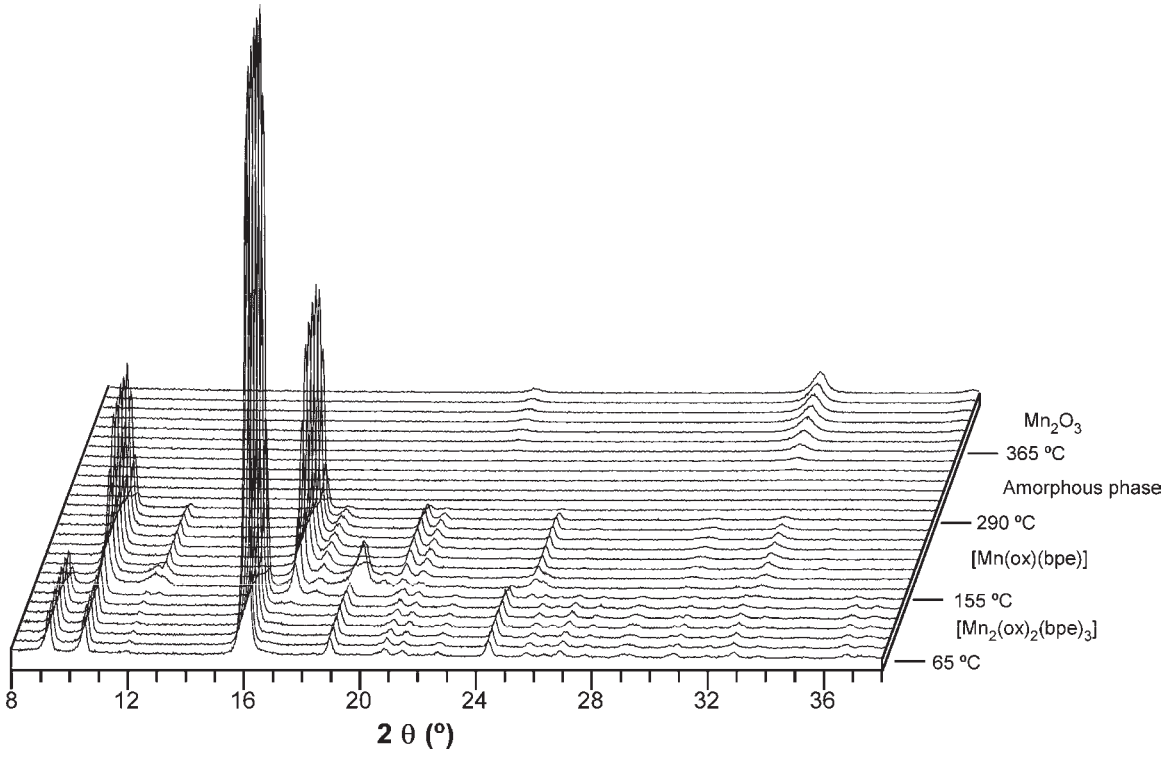

Figure 7. Variable-temperature X-ray powder diffraction patterns of compound **3**.

room temperature up to 215 °C at a constant rate of 5 °C/min. Although the elemental analysis and IR spectroscopy agree with the formula [Mn(ox)(bpe)], the X-ray powder diffraction pattern was completely different, indicating the isolation of a new phase, **4b**. Compound **4b** is only obtained when a heating program similar to that which takes place during the TDX is applied. On the other hand, the diffraction patterns of compounds **4a** and **4b** differ also from those previously reported for analogous [M(ox)(bpe)], M being Fe, Co, Ni, Cu, and Zn (Figure 8a).[13]

Taking into account the broken ladder-like structure of starting compound **3** and the rectangular 2D network present in other [M(ox)(bpe)] systems, it is reasonable to expect a 2D crystal structure for compounds **4a** and **4b** (Figure 9). The main difference between them is the disposition of the sheets on the crystal structure. Depending on the heating rate, the system can acquire

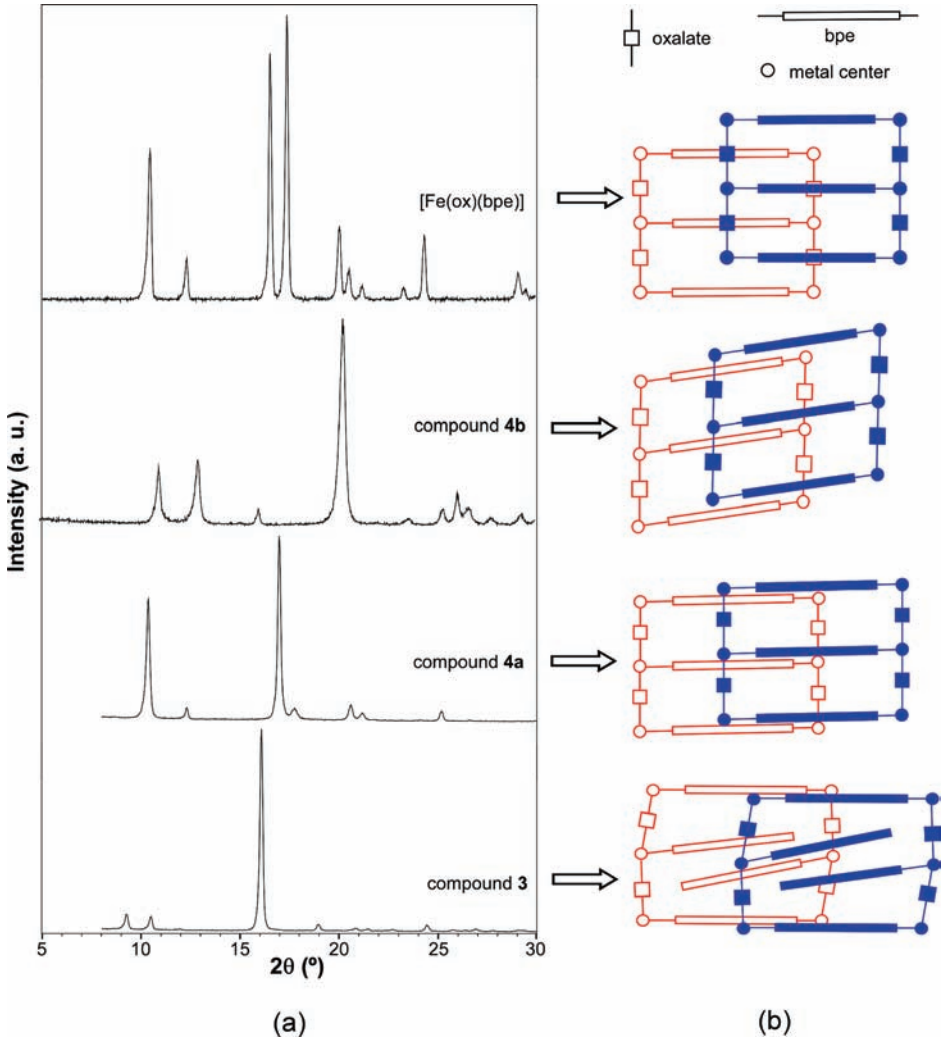

Figure 8. (a) X-ray powder diffraction patterns of compounds **3**, **4a**, **4b**, and [Fe(ox)(bpe)]. (b) Schematic representations of the relative arrangement of the polymeric sheets in each compound.

enough energy to surpass the energy barriers present during the rearrangement of the sheets. In fact, intermediate heating rates give rise to mixtures of compounds **4a** and **4b**.

The cell parameters obtained for compounds **4a** and **4b** could be easily related to the M···M distances through the oxalato and bpe bridging ligands. It allows us to draw a schematic description of the structures in which we can observe that the hydrogen bonding interaction among the bpe entities and the oxalato ligand takes place with just one of the coordinated oxygen atoms, so the bpe ligand is placed at one side of the oxalato ligand. The same disposition between the oxalato and bpe ligands is found in the starting compound **3**. In the related [M(μ-ox)(μ-bpe)] (M^{II} = Fe, Co, Ni, Cu, and Zn) compounds, the interaction takes place simultaneously with two oxygen atoms of the same oxalato ligand through a bifurcated hydrogen bond, and as a consequence, the bpe molecule is placed just above the middle of the oxalato ligand. It indicates that during the thermal treatment, the supramolecular interactions present on the starting material direct the crystal structure of the resulting compound toward a thermodynamically unstable crystal structure which is more closely related to the starting crystal structure.

It is worth noting that the angle between the oxalato and bpe bridging ligands in compound **3** is similar to that found when the sample is rapidly heated: compound **4b** (*ca.* 100°). In the case of compound **4a**, which is obtained when a prolonged heating process takes place, a value of *ca.* 92° is presented, closer to that observed on the previously reported [M(μ-ox)(μ-bpe)] compounds (90°).

Crystal Structure of $\{[Mn_4(\mu\text{-ox})_3(\mu\text{-bpe})_4(H_2O)_4]\cdot(X)_2\cdot mY\}_n$ (X = NO_3^- for 5a, Br^- for 5b, and ClO_4^- for 5c; Y = Solvation Molecules). Each metal center in compounds **5a** and **5b** has a pentagonal bipyramid O_5N_2 donor set in which the basal plane is formed by five O atoms from one water molecule and two oxalato anions, whereas the bpe ligands are located in the axial positions (Figure 10). Selected bond lengths and angles are gathered in Table 5. The tris-bidentate ox1 anion sequentially bridges Mn1 atoms to form corrugated chains that run parallel to the *b* axis and Mn2 metal centers with one carboxylic group through O11 and O12 atoms, forming a μ-oxo bridge. Bis-bidentate ox2 ligands connect Mn2 atoms between them, building $[Mn_4(ox)_3(H_2O)_4]^{2+}$ sheets in the plane *bc* (Figure 11a). It is noteworthy that $Mn-O_{ox}$ distances that imply μ-oxo bridge oxygen atoms are substantially longer (> 2.38 Å) than those that are not involved (< 2.27 Å).

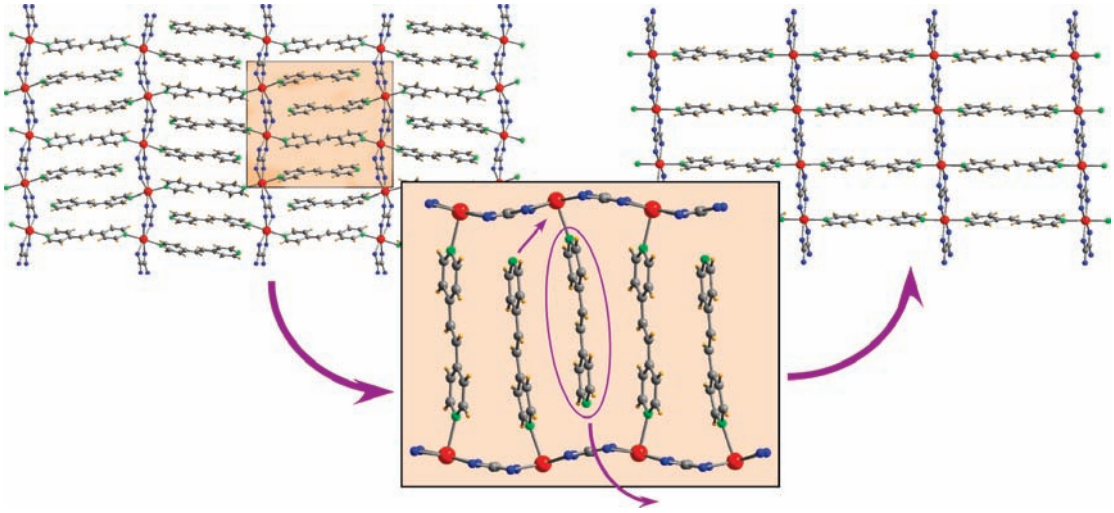

Figure 9. Representation of the rearrangement process taking place within the sheets in compound **3** during the bpe molecule's release.

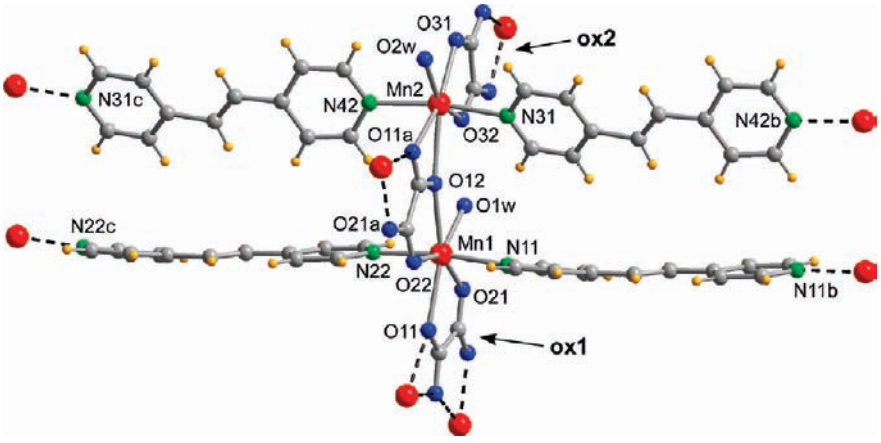

Figure 10. Fragment of the molecular net for compounds **5a** and **5b** with the atom numbering scheme. Symmetry codes: (a) $-2-x, 1/2+y, 1/2-z$; (b) $-1+x, y, z$; (c) $1+x, y, z$.

The *trans*-coordinated bpe ligands bridge metal centers of consecutive sheets constructing the three-dimensional cationic net $[Mn_4(ox)_3(H_2O)_4(bpe)_4]^{2+}$, as shown in Figure 11c. These molecules are perpendicular to the 2D Mn−ox framework (with angles higher than 80° between the pyridinic rings and the *bc* plane), generating cylindrical channels along the *a* axis (d ∼ 6 Å) and rectangular ones parallel to the *b* axis (4 × 13 Å), which lends a high porosity to the structure. An empty volume per unit cell of 1275.3 $Å^3$ (32.6%) and 1092.8 $Å^3$ (28.5%) has been calculated for compounds **5a** and **5b**, respectively. The guest molecules placed on the channels of both compounds could not be crystallographically located and were determined by elemental analyses and TG/DTA measurements.

The crystal structure is completed with the presence of nitrate, bromide, or perchlorate anions that counterbalance the charge of the metal−organic framework. The anions are placed on specific voids of the net (Supporting Information) in which three bpe ligands are orientated to the anions holding them by hydrogen bonds.

The loss of guest molecules takes place from room temperature to 160 and 175 °C for compounds **5a** and **5b**, respectively. The weight loss has been attributed to 10 water molecules for compound **5a** (exptl, 11.65%; calcd, 11.34%) and to five water and four methanol molecules for **5b** (exptl, 13.20%; calcd, 13.14%). The remaining molecular framework is stable up to 240 °C (**5a**) and 220 °C (**5b**), when the coordinated water molecules are released with the breakdown of the overall structure leading to the formation of Mn_2O_3 as a final residue. The decomposition process takes place through successive processes in which the anion influences the thermal stability of the complex, as is proved by the difference in the temperature range of the process, 105 °C for **5a** and 175 for **5b**.

Ion Exchange. The capability to exchange the host anions in the open structure of compounds **5a**, **5b**, and **5c** was analyzed by FTIR and powder X-ray diffraction (Supporting Information). Powder samples of the compounds (0.1 g) were added to 0.1 M solutions of KBr, $NaClO_4$, or KNO_3 at room temperature and stirred for different time periods. The ion exchange could be easily determined by FTIR because the signals of the anions used in the experiments appear at different values: an intense peak at 1385 cm^{-1} for the nitrate anion; three signals at 1120, 1090, and 625 cm^{-1} for the perchlorate anion; and no signal for the bromide ion. Powder X-ray diffraction showed that during the ion exchange the crystal structure of the compounds is retained.

Table 5. Selected Bond Lengths (Å) and Angles (deg) for Compounds **5a** and **5b**[a]

	5a	5b		5a	5b
Mn(1)−O(11)	2.378(2)	2.379(4)	Mn(2)−O(11a)	2.446(2)	2.446(4)
Mn(1)−O(12)	2.400(2)	2.416(4)	Mn(2)−O(12)	2.447(2)	2.460(4)
Mn(1)−O(21)	2.226(2)	2.265(5)	Mn(2)−O(31)	2.248(2)	2.266(4)
Mn(1)−O(22)	2.202(2)	2.225(4)	Mn(2)−O(32)	2.200(2)	2.228(5)
Mn(1)−N(11)	2.261(3)	2.285(5)	Mn(2)−N(31)	2.244(3)	2.262(6)
Mn(1)−N(22)	2.243(3)	2.269(5)	Mn(2)−N(42)	2.243(3)	2.262(6)
Mn(1)−O(1w)	2.176(2)	2.188(4)	Mn(2)−O(2w)	2.155(2)	2.143(5)
O(11)−Mn(1)−O(12)	144.7(1)	145.1(2)	O(11)a−Mn(2)−O(12)	53.0(1)	52.9(1)
O(11)−Mn(1)−O(21)	70.8(1)	70.6(2)	O(11)a−Mn(2)−O(31)	157.3(1)	157.7(2)
O(11)−Mn(1)−O(22)	74.4(1)	75.2(2)	O(11)a−Mn(2)−O(32)	130.1(1)	130.1(2)
O(11)−Mn(1)−N(11)	87.4(1)	86.8(2)	O(11)a−Mn(2)−N(31)	87.7(1)	87.9(2)
O(11)−Mn(1)−N(22)	84.8(1)	84.9(2)	O(11)a−Mn(2)−N(42)	84.5(1)	84.0(2)
O(12)−Mn(1)−O(21)	144.5(1)	144.2(1)	O(12)−Mn(2)−O(31)	149.6(1)	149.4(2)
O(12)−Mn(1)−O(22)	70.4(1)	70.0(1)	O(12)−Mn(2)−O(32)	77.1(1)	77.3(1)
O(12)−Mn(1)−N(11)	92.2(1)	93.2(2)	O(12)−Mn(2)−N(31)	84.6(1)	84.4(2)
O(12)−Mn(1)−N(22)	92.8(1)	92.3(2)	O(12)−Mn(2)−N(42)	86.9(1)	86.0(2)
O(21)−Mn(1)−O(22)	145.2(1)	145.8(2)	O(31)−Mn(2)−O(32)	72.5(1)	72.2(2)
O(21)−Mn(1)−N(11)	90.2(1)	89.8(2)	O(31)−Mn(2)−N(31)	95.0(1)	93.6(2)
O(21)−Mn(1)−N(22)	89.4(1)	89.6(2)	O(31)−Mn(2)−N(42)	94.1(1)	96.1(2)
O(22)−Mn(1)−N(11)	87.3(1)	87.8(2)	O(32)−Mn(2)−N(31)	89.9(1)	90.5(2)
O(22)−Mn(1)−N(22)	88.5(1)	88.0(2)	O(32)−Mn(2)−N(42)	91.4(1)	90.2(2)
N(11)−Mn(1)−N(22)	171.9(1)	171.4(2)	N(31)−Mn(2)−N(42)	170.8(1)	170.0(2)
O(1w)−Mn(1)−O(11)	142.6(1)	141.7(2)	O(2w)−Mn(2)−O(11)a	76.8(1)	77.5(2)
O(1w)−Mn(1)−O(12)	72.6(1)	73.1(2)	O(2w)−Mn(2)−O(12)	129.8(1)	130.4(1)
O(1w)−Mn(1)−O(21)	71.9(1)	71.1(2)	O(2w)−Mn(2)−O(31)	80.6(1)	80.2(2)
O(1w)−Mn(1)−O(22)	142.9(1)	143.1(2)	O(2w)−Mn(2)−O(32)	153.1(1)	152.4(2)
O(1w)−Mn(1)−N(11)	94.6(1)	94.2(2)	O(2w)−Mn(2)−N(31)	92.0(1)	92.2(2)
O(1w)−Mn(1)−N(22)	93.0(1)	93.7(2)	O(2w)−Mn(2)−N(42)	90.9(1)	91.8(2)

[a] Symmetry code: (a) $-2 - x$, $1/2 + y$, $1/2 - z$.

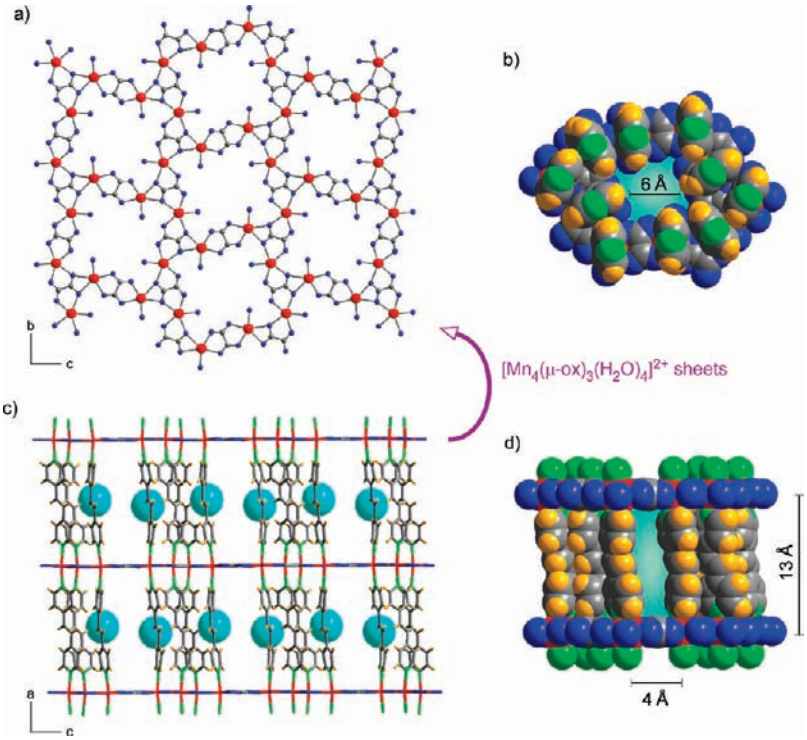

Figure 11. (a) Mn−ox sheets in the *bc* plane. (b) Space-filling picture of the channels parallel to the *a* axis. (c) Three-dimensional metal−organic network for compound **5b**. The blue spheres represent the location of the anions in the structure. (d) Space-filling picture of the rectangular channels parallel to the *b* axis.

In conclusion, we can confirm that the exchange between the three anions along the channels is possible without a loss of the initial 3D structure. The mobility of the anions decreases in the following order: NO_3^- > Br^- > ClO_4^-. The nitrate anion could be easily replaced by bromide or perchlorate anions, and after 24 h the exchange is completed. The substitution of the bromide anions by nitrate ones was also fast, but only a partial replacement of bromide by perchlorate anions could be obtained after 6 days. Finally, the perchlorate ions were only partially exchanged by nitrate or bromide anions. These facts seem to indicate a selectivity of the holes for

Table 6. Relevant Magnetic Data for Compounds **1**−**3** and **5** Including the Curie−Weiss Law Fitting

compound	$\chi_M T$[a]	$\chi_M \times 10^{2}$[b]	T_1 (K)[c]	$\chi_M \times 10^{2}$[d]	T_2 (K)[e]	ΔT (K)[f]	C[g]	θ (K)
1	4.12	7.4	19			50−300	4.54	−29.4
2	4.14	10.2	13			30−300	4.50	−23.1
3	4.48	9.2	15			40−300	4.92	−29.2
5a	8.11	17.5	6.0	17.2	3.2	40−300	9.05	−34.8
5b	8.21	19.5	4.7	19.4	4.2	40−300	9.16	−35.2
5c	8.22	18.9	5.5	18.3	3.0	40−300	9.14	−31.4

[a] Room temperature $\chi_M T$ value ($cm^3\ mol^{-1}\ K$). [b] Maximum value of the χ_M curve ($cm^3\ mol^{-1}$). [c] Temperature of the maximum of the χ_M curve. [d] Minimum value of the χ_M curve ($cm^3\ mol^{-1}$). [e] Temperature of the minimum of the χ_M curve. [f] Range of the Curie−Weiss fitting. [g] Units: $cm^3\ mol^{-1}\ K$.

the shape and size of the anions. We tried the replacement of the anions by smaller ones such as Cl^- or bigger ones such as BF_4^- and PF_6^-, but no results were obtained. It is worth highlighting that although the bromide ion is smaller than the nitrate ion, its mobility was lower, showing a shape dependence in the exchange process.

Magnetic Properties. The temperature dependence of the molar magnetic susceptibility (χ_M) for compounds **1**−**3** and **5** increases upon cooling up to a maximum around 15 K for complexes **1**−**3** and 5 K for **5a**−**5c** (Table 6). The room temperature value of $\chi_M T$ for compounds **1**−**3** is similar to the spin-only value expected for a high-spin d^5 Mn(II) ion (4.38 $cm^3\ mol^{-1}\ K$, considering $g = 2.00$) and for two Mn(II) ions for complexes **5a**−**5c**. The thermal variation of the χ_M^{-1} for all compounds could be described by the Curie−Weiss law, obtaining in all cases a negative value for θ. All of these facts are indicative of the presence of predominant antiferromagnetic interactions between the metal centers.

Additionally, the χ_M curve for compounds **5a**−**5c** shows a local minimum below 4 K (Figure 12), which can be due to a ferromagnetic ordering of the network at low temperatures (spin canting). Attending to the crystal structure, these compounds can be described as magnetic metal−oxalato sheets joined by bpe ligands. As can be observed in Figure 13, these 2D magnetic structures are built up by triangular Mn(II) fragments forming chains along the *b* axis and connected by a bis-bidentate oxalato. The manganese atoms are bridged by a μ_3-oxalate anion with two magnetic paths: its usual bis-bidentate coordination mode, which shows values for the magnetic coupling (J_2) ranging from −0.81 to $-3.0\ cm^{-1}$ (Table 7), and the μ-O bridge (J_1) with *J* values of *ca.* $-3.0\ cm^{-1}$ for a M−O−M angle of 150−155°,[36] similar to that observed for compounds **5a**−**5c** (154−155°). The presence of these triangular fragments with similar antiferromagnetic *J* values implies that the magnetic moments cannot be completely coupled obtaining non-null magnetic values at low temperatures.

Figure 14 shows the thermal evolution of the χ_M and the $\chi_M T$ products of compounds **2** and **3**. These compounds can be considered, from a magnetic point of view, as 1D

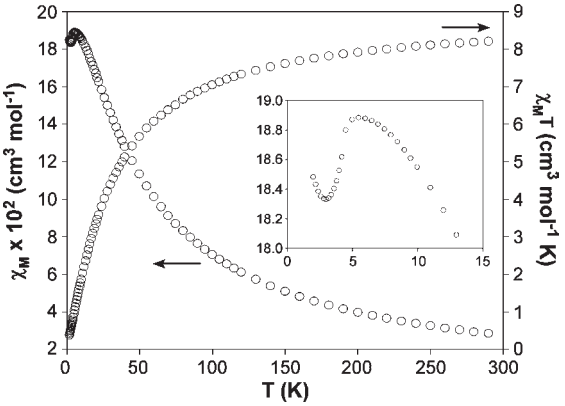

Figure 12. Thermal dependence of χ_M and $\chi_M T$ product for compound **5c**.

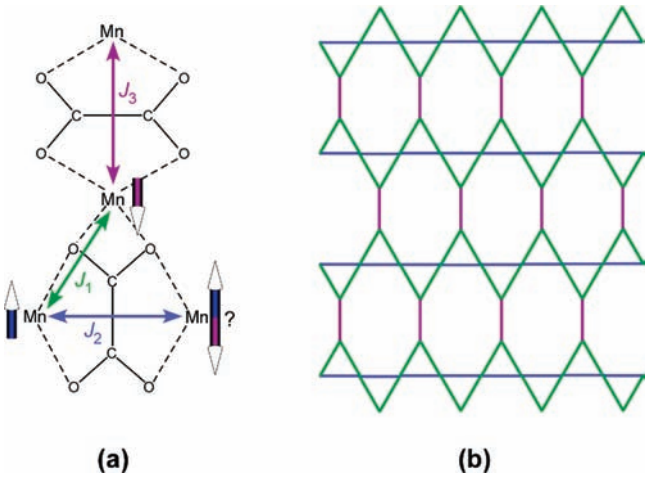

Figure 13. (a) Magnetic interactions in compounds **5a**−**5c** through the oxalato bridges. (b) Schematic representation of the 2D magnetic framework.

due to the long M···M distances (> 13 Å) along the bpe molecules that allow for an assumption of a negligible magnetic exchange through the organic ligands[37] and for analysis of their magnetic properties on the basis of a chain model. The experimental data have been successfully fitted by means of an $S = 5/2$ Fisher antiferromagnetic chain model derived through the Hamiltonian $H = -J \sum S_i S_{i+1}$.[38] The best fit parameters are $J = -2.43\ cm^{-1}$, $g = 2.00$, and $R = 7.4 \times 10^{-7}$ for **2** and $J = -2.16\ cm^{-1}$, $g = 2.00$, and $R = 6.4 \times 10^{-7}$ for **3** (solid line in Figure 14), where *R* is the agreement factor defined as $R = \sum_i (\chi_M)_{obs}(i) - (\chi_M)_{calcd}(i)]^2 / \sum_i (\chi_M)_{obs}(i)]^2$.

The *J* values of compounds **2** and **3** are in the range found for other reported oxalato-bridging manganese(II) complexes, which show a weak antiferromagnetic coupling ranging from −0.81 to $-3.00\ cm^{-1}$. Table 7 includes the magnetostructural data of previously reported Mn(II) compounds in which the magnetic interaction is transmitted by bis-bidentate oxalato ligands. The exchange pathway for this significant antiferromagnetic interaction is well-known[9a,39] and takes place between the $d_{x^2-y^2}$ type

(36) (a) Sun, Z.; Gantzel, P. K.; Hendrickson, D. N. *Polyhedron* **1998**, *17*, 1511. (b) Huang, D.; Wang, W.; Zhang, X.; Chen, C.; Chen, F.; Liu, Q.; Liao, D.; Li, L.; Sun, L. *Eur. J. Inorg. Chem.* **2004**, 1454.

(37) (a) Manna, S. C.; Zangrando, E.; Drew, M. G. B.; Ribas, J.; Chaudhuri, N. R. *Eur. J. Inorg. Chem.* **2006**, 481. (b) Ghosh, A. K.; Ghoshal, D.; Zangrando, E.; Ribas, J.; Chaudhuri, N. R. *Inorg. Chem.* **2005**, *44*, 1786. (c) Mukhopadhyay, S.; Chatterjee, P. B.; Mandal, D.; Mostafa, G.; Caneschi, A.; Van Slageren, J.; Weakley, T. J. R.; Chaudhury, M. *Inorg. Chem.* **2004**, *43*, 3413.

(38) Fisher, M. E. *Am. J. Phys.* **1964**, *32*, 343.

(39) (a) Julve, M.; Verdaguer, M.; Kahn, O.; Gleizes, A.; Philoche-Levisalles, M. *Inorg. Chem.* **1983**, *22*, 368. (b) Julve, M.; Verdaguer, M.; Gleizes, A.; Philoche-Levisalles, M.; Kahn, O. *Inorg. Chem.* **1984**, *23*, 3808.

Table 7. Magnetostructural Data (Å, cm^{-1}) for Oxalato-Bridged Mn(II) Complexes[a]

compound[b]	type	D_{Mn}	h	γ	S_{oc}	S_{tp}	g	J	ref
			trans-MnO_6						
$[Mn(\mu\text{-ox})(H_2O)_2]_n$[c]	1D	5.63					2.00	−0.88	43, 44
$[Mn(\mu\text{-ox})(D_2O)_2]_n$	1D	5.65	0.00	0.1	0.86	15.82	2.00	−0.81	43
$[Mn(\mu\text{-ox})(dpyo)]_n$	2D	5.66	0.00	0.0	0.97	15.94	2.00	−1.89	37a
			cis-MnO_6						
$\{[Mn(\mu\text{-ox})(H_2O)_2]\cdot(H_2O)\}_n$	1D	5.71	0.10	9.5	2.15	8.75	2.02	−1.07	45
$\{[Mn(\mu\text{-ox})(H_2O)_2]\cdot(ade)\cdot(H_2O)\}_n$	1D	5.70	0.12/0.06	9.6/9.5	1.30	11.18	2.00	−1.82	12b
			cis-MnO_5N						
$[Mn(\mu\text{-ox})(pur)(H_2O)]_n$	1D	5.60	0.21/0.29	6.1/13.2	1.07	12.53	2.00	−1.99	12b
			trans-MnO_4N_2						
$[Mn(\mu\text{-ox})(4atr)_2]_n$	1D	5.60	0.26	8.6	0.89	15.74	2.00	−1.74	11b
$[Mn(\mu\text{-ox})(bpa)]_n$	2D	5.59	0.34	15.8	0.98	14.82	2.00	−1.91	13
$[Mn_2(\mu\text{-ox})_2(\mu\text{-bpe})(bpe)_2]_n$	2D	5.54	0.21/0.57	3.7/22.5	2.27	10.82	2.00	−2.16	*d*
			cis-MnO_4N_2						
$[Mn(\mu\text{-ox})(\mu\text{-bpm})]_n$	2D	5.61	0.07	12.3/13.2	3.16	7.51	1.99	−3.00	46
$[Mn(\mu\text{-ox})(bpy)]_n$	1D	5.62	0.07	11.0/13.6	2.39	9.93	1.97	−2.40	47
$[Cr_2Mn_2(ox)_5(phen)_2(bpy)_2(H_2O)_2]\cdot 6H_2O$[e]	tetramer	5.70	0.09	9.5	1.89	11.41	1.99	−2.20	48
			0.13	10.9	1.62	11.21			
$[Mn(\mu\text{-ox})(bpe)]_n$	3D	5.68	0.09/0.12	6.7/8.1	2.27	10.75	2.00	−2.43	*d*
			MnO_3N_3						
$[Mn_2(\mu\text{-ox})(bpppa)_2](ClO_4)_2$[e]	dimer	5.63	0.07/0.11	10.4/23.1	6.17	5.05	2.00	−2.95	9c
					9.00	2.21			
			MnO_2N_4						
$\{Mn(\mu\text{-ox})_{0.5}(bpy)[Cr(bpy)(CN)_4]\}_n$[f]	dimer	5.68	0.06	3.1	1.94	10.15	2.07	−1.20	49
$[Mn_2(\mu\text{-ox})(bispicen)_2](ClO_4)_2$[e]	dimer	5.63	0.08	2.0	3.37	9.14	2.02	−1.91	46
			0.21	11.2	4.01	10.70			
$[Mn_2(\mu\text{-ox})(bisMe_2picen)_2](ClO_4)_2$	dimer	5.61	0.11	14.4	2.64	9.18	1.99	−2.04	46
$[Mn_2(\mu\text{-ox})(bispictn)_2](ClO_4)_2$[c]	dimer						2.01	−2.48	46

[a] The table includes only those examples in which only a crystallographically independent metal center and oxalato bridging ligand are present. Abbreviations used, D_{Mn}: metal−metal distance. h: displacement of the manganese atom out of the basal plane. γ: dihedral angle between the equatorial and oxalato mean planes. S_{oc}: octahedral distortion. S_{tp}: trigonal prism distortion. dpyo = 4,4′-bipyridine-N,N′-dioxide; ade = adenine; pur = purine; bpm = 2,2′-bipyrimidine; bpy = 2,2′-bipyridine; phen = 1,10-phenanthroline; bpe = bis(4-pyridyl)ethylene; titmb = 1,3,5-tris(imidazol-1-ylmethyl)-2,4,6-trimethylbenzene; 4atr = 4-amino-1,2,4-triazole; bpa = bis(4-pyridyl)ethane; bpppa = N-benzyl-N-((6-pivaloylamido-2-pyridyl)methyl)-N-(2-pyridylmethyl)amine; bispicen = N,N′-bis(2-pyridylmethyl)-1,2-ethanediamine; bisMe$_2$picen = N,N′-bis(2-pyridylmethyl)-N,N′-dimethyl-1,2-ethanediamine; bispictn = N,N′-bis(2-pyridylmethyl)-1,3-propanediamine. [b] *cis* and *trans* conformations correspond to the relative orientation of the oxalato ligands in the polymeric compounds. [c] Structure not reported. Mn···Mn distance of the first compound was determined by the corresponding crystallography axis of the powder X-ray diffraction. [d] This article. [e] More than one crystallographically independent Mn(II) atom reported in the structure. [f] Although a 1D structure, oxalato bridges join heterometal−cyanide squares, and they can be considered, for our study, dimeric units. The table includes only those examples in which only a crystallographically independent metal center and oxalate bridging ligand are present.

metal magnetic orbitals and the bridging-ligand σ orbitals in the dimeric entities.[40] The x and y axes of the metal orbitals are defined by the Mn−O_{ox} bonds, which implies that the Mn···Mn distance is a very important factor in the magnitude of the magnetic exchange coupling. It means that lower metal distances involve a higher orbital overlap and consequently higher $|J|$ values, as shown in Table 7.

Also, structural distortions such as deviations from the planarity of the metal ion with respect to the mean plane of the bridging ligand (h) or the dihedral angle of this plane with the equatorial one (γ) play a key role in the fine-tuning of the exchange coupling.[39,41] In different oxalato-bridged nickel(II) compounds, it has been observed that an increase in the electronegativity of the donor atoms in the peripheral ligands reduces the antiferromagnetic coupling through the oxalato bridge. This trend is more notorius if the most electronegative donor atom is coplanar with the bridging ligand than if it is axially located.[9a,10a,41a,42] As can be observed in Table 7, the coordination environment is an important factor in the nature of the magnetic coupling of the oxalato-bridged Mn(II) compounds. The lowest J values have been reported for the MnO_6 chromophore ($-0.81 < J < -1.89$ cm^{-1}). The O_4N_2 donor set presents values near -2.0 cm^{-1} when both nitrogen atoms are axially coordinated and above -2.2 cm^{-1} if a nitrogen atom occupies an axial position and the other one the equatorial. However,

(40) Glerup, J.; Goodson, P. A.; Hodgson, D. J.; Michelsen, K. *Inorg. Chem.* **1995**, *34*, 6255.

(41) (a) Cano, J.; Alemany, P.; Alvarez, S.; Verdaguer, M.; Ruiz, E. *Chem.—Eur. J.* **1998**, *4*, 476. (b) Bordas, E.; Caballol, R.; de Graaf, C. *THEOCHEM* **2005**, *727*, 173. (c) Alvarez, S.; Julve, M.; Verdaguer, M. *Inorg. Chem.* **1990**, *29*, 4500. (d) Cabrero, J.; Amor, N. B.; de Graaf, C.; Illas, F.; Caballol, R. *J. Phys. Chem. A* **2000**, *104*, 9983.

(42) Vitoria, P.; Muga, I.; Gutiérrez-Zorrilla, J. M.; Luque, A.; Román, P.; Lezama, L.; Zúñiga, J.; Beitia, J. I. *Inorg. Chem.* **2003**, *42*, 960.

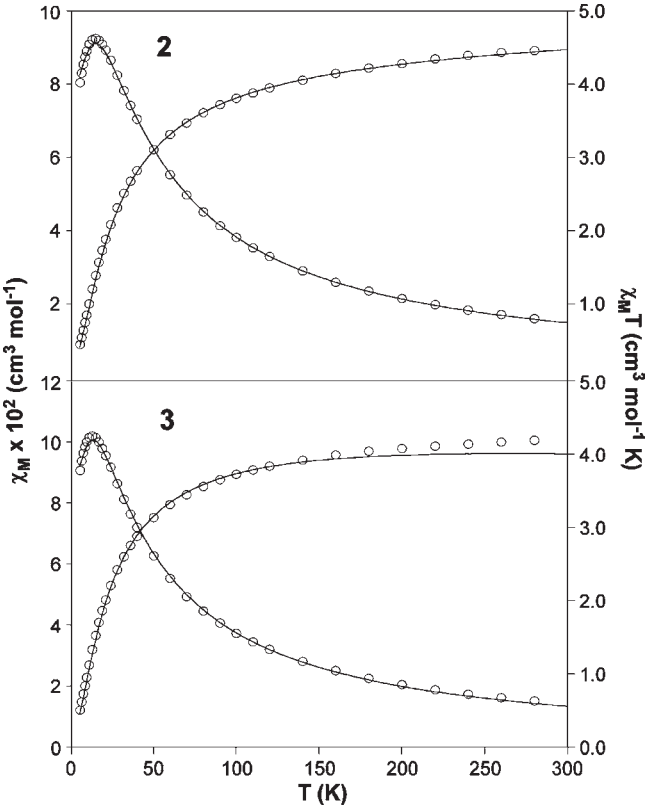

Figure 14. Thermal dependence of χ_M and $\chi_M T$ products for compounds **2** (up) and **3** (down). The solid line represents the best fit curve.

several dimeric entities with a MnO_2N_4 environment show J values ranging from -1.2 to $+2.5$ cm^{-1}, lower than those expected for this chromophore, which implies that other factors such as structural parameters and distortions must also be taken into account.

Figure 15 shows the decrease of the magnetic coupling with the Mn···Mn distance along the oxalato bridge, but in a deep analysis it has been observed that *trans*-coordinated oxalato ligands provide lower $|J|$ values than the *cis*-coordinated ones with similar metal−metal distances, while dimeric entities present values between the previous ones. This trend is expected for polymeric compounds with a MnO_4N_2 chromophore, because *trans* complexes present two nitrogen atoms in axial positions, while for *cis*-coordinated complexes, one N atom is axial and the other one equatorial, which implies higher values according to the previously discussed ones. But the fact that the O_6 donor set also follows this trend seems to indicate that the relative orientation of the bridged ligands between them is more relevant for the magnetic coupling than the electronegativity of the peripheral ligands. Indeed, the MnO_2N_4 dimeric entities have lower values than the polymeric

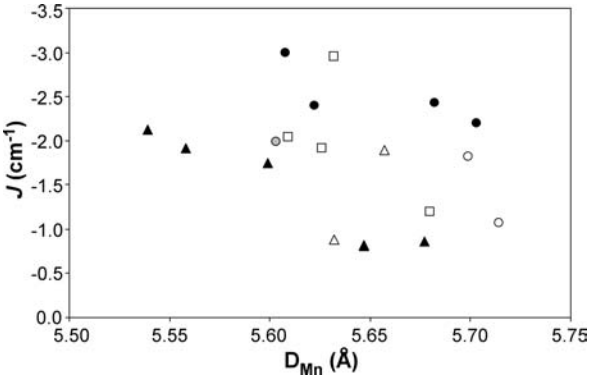

Figure 15. Dependence of the magnetic coupling value on the manganese atoms distance through the oxalato bridge (D_{Mn}). Circle = *cis*-coordinated oxalato ligands, triangle = *trans*-coordinated oxalato ligands, square = dimeric entities, open = MnO_6 chromophore, black solid = MnO_4N_2 chromophore, gray solid = MnO_5N chromophore.

cis-coordinated compounds although they have more N atoms in the coordination sphere of the metal.

To study in depth the different structural parameters that influence the magnetic properties of the oxalato-bridged Mn(II) compounds, we have analyzed the distortion of the metal polyhedron on the basis of the continuous shape measures (CShM). Avnir and co-workers[50] defined "symmetry measures" to quantify the degree of distortion of the metal environment from an ideal polyhedron, it means a quantitative measure of the minimal distance to the desired perfect symmetry (S_x). A useful tool for analysis of families of compounds is the scatterplots of their shape measures over the interconversion path between the two ideal polyhedra with the same number of vertices, which are called "shape maps".[51] Obviously, these measures take into account all possible structural factors that influence the distortion of the polyhedra, giving an overall single parameter, but the CShM has found many novel correlations between symmetry or chirality and molecular properties.[52] In our case, all compounds present a hexacoordinated metal environment, the octahedron (O_h) and trigonal prism (D_{3h}) being the most common polyhedra. The characteristic distortion that interconverts these two ideal polyhedra is the Bailar twist,[53] which allows calculation of their shape map.[54] Figure 16 shows the pathway between the two ideal polyhedra and the calculated symmetry measures for the octahedral [$S(O_h)$] and trigonal prism [S(tp)] coordination sphere of the experimental structures using the program SHAPE,[55] which can be obtained from the authors upon request.

(43) Mitsuda, S.; Simizu, S.; Lukin, J.; Friedberg, S. A.; Yang, B. X.; Shirane, G. *Phys. Rev. B* **1988**, *38*, 9035.
(44) Deyrieux, R.; Berro, C.; Peneloux, A. *Bull. Soc. Chim. Fr.* **1973**, 25.
(45) Wu, W.-Y.; Song, Y.; Li, Y.-Z.; You, X.-Z. *Inorg. Chem. Commun.* **2005**, *8*, 732.
(46) De Munno, G.; Ruiz, R.; Lloret, F.; Faus, J.; Sessoli, R.; Julve, M. *Inorg. Chem.* **1995**, *34*, 408.
(47) Deguenon, D.; Bernardinelli, G.; Tuchagues, J. P.; Castan, P. *Inorg. Chem.* **1990**, *29*, 3031.
(48) Marinescu, G.; Andruh, M.; Lescouëzec, R.; Muñoz, M. C.; Cano, J.; Lloret, F.; Julve, M. *New J. Chem.* **2000**, *24*, 527.
(49) Zhang, Y.-Z.; Wang, Z.-M.; Gao, S. *Inorg. Chem.* **2006**, *45*, 5447.
(50) Zabrodsky, H.; Peleg, S.; Avnir, D. *J. Am. Chem. Soc.* **1992**, *114*, 7843.
(51) (a) Pinsky, M.; Avnir, D. *Inorg. Chem.* **1998**, *37*, 5575. (b) Casanova, D.; Cirera, J.; Llunell, M.; Alemany, P.; Avnir, D.; Alvarez, S. *J. Am. Chem. Soc.* **2004**, *126*, 1755. (c) Alvarez, S.; Alemany, P.; Casanova, D.; Cirera, J.; Llunell, M.; Avnir, D. *Coord. Chem. Rev.* **2005**, *249*, 1693.
(52) (a) Keinan, S.; Avnir, D. *J. Chem. Soc., Dalton Trans.* **2001**, 941. (b) Katznelson, O.; Edelstein, J.; Avnir, D. *Tetrahedron: Asymmetry* **2000**, *11*, 2695. (c) Zabrodsky, H.; Avnir, D. *J. Am. Chem. Soc.* **1995**, *117*, 462. (d) Alvarez, S.; Pinsky, M.; Avnir, D. *Eur. J. Inorg. Chem.* **2001**, 1499. (e) Alvarez, S.; Llunell, M. *J. Chem. Soc., Dalton Trans.* **2000**, 3288.
(53) Bailar, J. C. *J. Inorg. Nucl. Chem.* **1958**, *8*, 165.
(54) Alvarez, S.; Avnir, D.; Llunell, M.; Pinsky, M. *New. J. Chem.* **2002**, *26*, 996.
(55) Llunell, M.; Casanova, D.; Cirera, J.; Bofill, J. M.; Alemany, P.; Alvarez, S.; Pinsky, M.; Avnir, D. *SHAPE* (1.1); Barcelona, 2003.

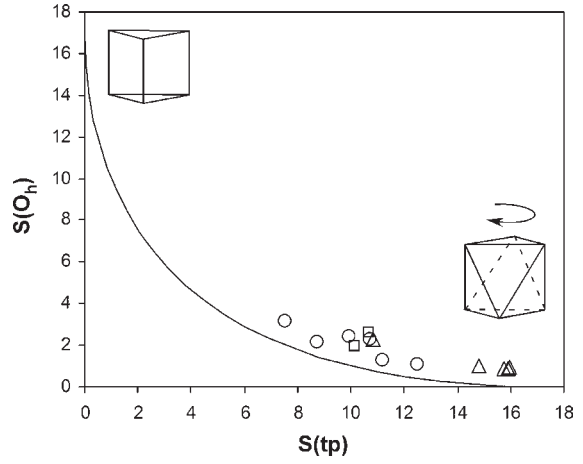

Figure 16. Octahedron-trigonal prism shape map of the experimental M(II)−oxalato structures. Solid line = ideal octahedron−trigonal prism interconversion pathway through bailar twist; circles = *cis*-coordinated oxalato ligands; triangles = *trans*-coordinated oxalato ligands; squares = dimeric entities.

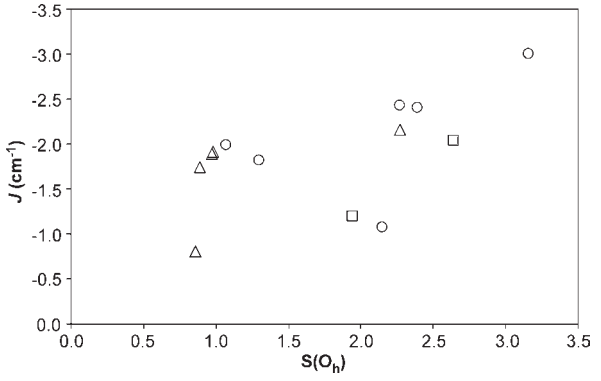

Figure 17. Relationship between the shape measures and the magnetic coupling constant in the oxalato-bridged Mn(II) complexes. Circles = *cis*-coordinated oxalato ligands; triangles = *trans*-coordinated oxalato ligands; squares = dimeric entities.

The first conclusion that we obtain is that most of the experimental compounds are octahedral with a slight distortion, and the lowest $S(O_h)$ values correspond to the *trans*-coordinated compounds. It has been determined that the intermediate geometry, isosymmetric with respect to the ideal octahedron and the trigonal prism, has $S(O_h) = S(\text{tp}) = 4.42$,[52e] a higher value than most of the experimental M(II)−oxalato shape measures. Second, it has been shown that the compounds appear along the Bailar path, despite the fact that the bite angle of the oxalato ligand and the presence of polydentate ligands could turn the experimental values away from the path.

Previously reported studies[52a,d] have shown different electronic and magnetic correlations with the CShM of different Cu(II) complexes. The representation of the experimental data with the shape measure (Figure 17, structures with different $S(O_h)$ values but only one magnetic coupling reported have been omitted) surprisingly shows a linear correlation in which the $|J|$ increases with the octahedral distortion. Further work is in progress to relate this magnetostructural correlation with the variations that take place on the electronic structure of the complexes.

Conclusions

In this paper, a family of extended metal(II)−oxalato compounds has been characterized from magnetic and structural points of view. This work emphasizes that, although using the same building blocks, several different crystal structures could be obtained just modifying the synthetic conditions: pH, stoichiometry, thermal treatment, and counterions. In this way, it has been demonstrated that the presence of counterions in the reaction media is crucial for the building process of charged multidimensional frameworks. The qualitative ion exchange experiments indicate that the shape and size of the anions placed on the channels play a major role in determining their relative mobility within these channels. The paper also pays special attention to the heating rate in the solid state transformation taking place in the broken ladder-like structure of compound **3** to provide two polymorphs with a 2D rectangular grid structure.

On the other hand, the continuous shape measurements realized in the metal polyhedra allow us to establish a magnetostructural relationship that depends on the degree of distortion of the metal environment with regard to ideal polyhedra. This magnetostructural correlation has the same relevance as that previously found for the Mn···Mn distance and, altogether with the chromophore type, could allow the prediction of the magnetic exchange for oxalato-bridged manganese(II) complexes.

Acknowledgment. Financial support from the Ministerio de Ciencia e Innovación (Project MAT2008−05690/MAT) and the Gobierno Vasco (IT477-10) is gratefully acknowledged. We also thank Universidad del País Vasco/Euskal Herriko Unibertsitatea for predoctoral fellowships (PIFA01/2007/021). Technical and human support provided by SGIker (UPV/EHU, MICINN, GV/EJ, ESF) is gratefully acknowledged.

Supporting Information Available: IR spectra, thermoanalytic curves, and noncovalent interactions for compounds **1**−**5**. XRPD analysis of compounds **4a**, **4b**, and **5c**. IR and XRPD monitorization of the ion exchange experiments in compounds **5a**, **5b**, and **5c**. Magnetic data of compounds **1**, **5a**, and **5b**. This material is available free of charge via the Internet at http://pubs.acs.org.